AD-A194 931 ENERGY CONVERSION MEASUREMENTS IN LASER-SUSTAINED ARGON 1/1
PLASMAS FOR APPLI (U) ILLINOIS UNIV AT URBANA DEPT OF
MECHANICAL AND INDUSTRIAL ENG H KRIER ET AL
UNCLASSIFIED 15 APR 88 UILU-ENG-88-4006 AFOSR-TR-88-0541 F/G 21/8 NL

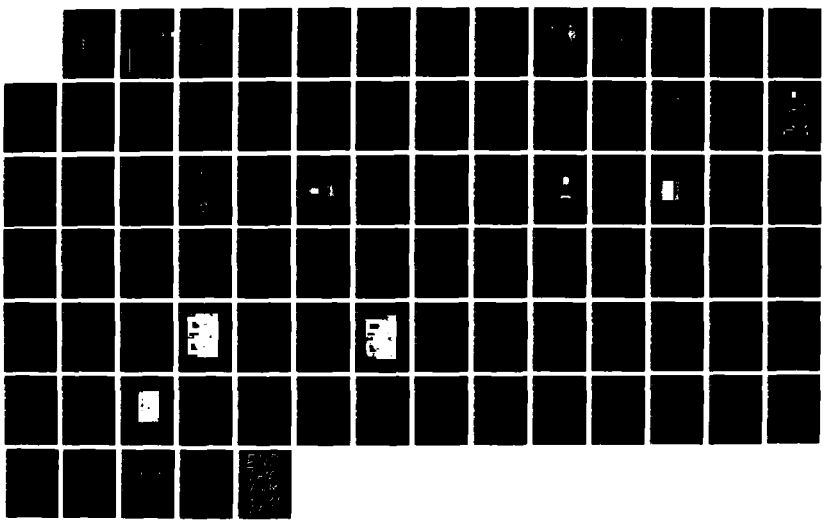

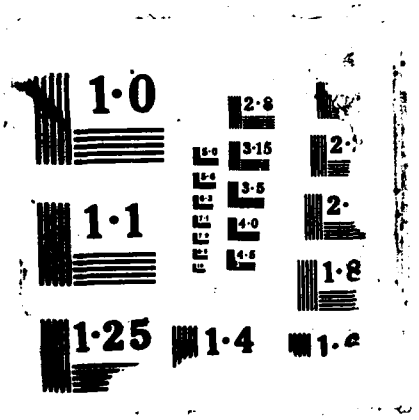
1·0
1·1
1·25
1·4
2·8
3·15
3·5
4·0
4·5
2·
2·
1·8

AFOSR-TR- 88-0

Department of Mechanical and
Industrial Engineering
University of Illinois at
Urbana-Champaign
Urbana, IL 61801

UILU ENG-88-4006

ENERGY CONVERSION MEASUREMENTS IN LASER-SUSTAINED ARGON PLASMAS FOR APPLICATION TO ROCKET PROPULSION

H. Krier and J. Mazumder
Co-Principal Investigators

and

D. K. Zerkle, A. Mertogul, and S. Schwartz
Graduate Research Assistants

FINAL

~~Annual~~ Technical Report submitted to
Air Force Office of Scientific Research
Dr. Mitat Birkan, Progam Manager
for research conducted
during the period
~~1 February 1987 to 15 March 1988~~
under
Grant No. AFOSR-87-0169

18FEB87 - 17FEB88

April 1988

Unclassified
SECURITY CLASSIFICATION OF THIS PAGE

REPORT DOCUMENTATION PAGE

Form Approved OMB No. 0704-0188

1a REPORT SECURITY CLASSIFICATION: Unclassified	1b RESTRICTIVE MARKINGS: NONE
2a SECURITY CLASSIFICATION AUTHORITY	3 DISTRIBUTION/AVAILABILITY OF REPORT: Approved for public release; distribution is unlimited
2b DECLASSIFICATION/DOWNGRADING SCHEDULE	
4 PERFORMING ORGANIZATION REPORT NUMBER(S): UILU-ENG-88-4006	5. MONITORING ORGANIZATION REPORT NUMBER(S): ~~AFOSR-TR~~ AFOSR-TR- 88-0541

6a NAME OF PERFORMING ORGANIZATION: University of Illinois at Urbana-Champaign	6b. OFFICE SYMBOL (If applicable): UIUC	7a. NAME OF MONITORING ORGANIZATION: AFOSR/NA	
6c ADDRESS (City, State, and ZIP Code): Dept. of Mechanical & Industrial Engineering 140 MEB; 1206 W. Green Street Urbana, IL 61801		7b. ADDRESS (City, State, and ZIP Code): Building 410, Bolling AFB DC 20332-6448	
8a NAME OF FUNDING/SPONSORING ORGANIZATION: AFOSR/NA	8b. OFFICE SYMBOL (If applicable): AFOSR	9. PROCUREMENT INSTRUMENT IDENTIFICATION NUMBER: AFOSR ~~Grant No~~. 87-0169	
8c. ADDRESS (City, State, and ZIP Code): Building 410, Bolling AFB DC 20332-6448		10. SOURCE OF FUNDING NUMBERS	
		PROGRAM ELEMENT NO.: 61102F	PROJECT NO.: 2308
		TASK NO: A1	WORK UNIT ACCESSION NO.

11. TITLE (Include Security Classification)
(U) Energy Conversion Measurements in Laser-Sustained Argon Plasmas for Application to Rocket Propulsion

12. PERSONAL AUTHOR(S)
H. Krier, J. Mazumder, D.K. Zerkle, A. Mertogul, S. Schwartz

13a. TYPE OF REPORT: ~~Annual~~ Technical	13b. TIME COVERED: FROM ~~2/1/87~~ TO ~~3/15/88~~	14. DATE OF REPORT (Year, Month, Day): ~~1988~~, April, 15	15. PAGE COUNT: 85

16. SUPPLEMENTARY NOTATION: 1 FEB 87 - 17 FEB 88

17. COSATI CODES		
FIELD	GROUP	SUB-GROUP

18. SUBJECT TERMS (Continue on reverse if necessary and identify by block number)
Beamed Energy Propulsion; Laser Plasma Formation

19. ABSTRACT (Continue on reverse if necessary and identify by block number)

Laser Propulsion is the production of high specific impulse rocket thrust using a high power laser as a remote energy source. Specific impulses in excess of 1000 seconds are achievable because propellant temperatures are very high and low molecular weight gases can be used. This report focuses on the energy conversion mechanisms of laser-sustained plasmas in flowing argon. The status of AFOSR sponsored experiments to determine thermal efficiency and global absorption is detailed. An improved testing facility has allowed plasma operating conditions never before possible. The results indicate that nearly all of the input laser power can be absorbed by a plasma. Plasmas at elevated gas pressure have been tested, and preliminary results presented. Optimal operating conditions have yet to be determined for the available laser powers and gas pressures. Further experimentation at very high argon gas velocities (> 20 m/s) must be performed in order to completely characterize plasma behavior.

(keywords)

[Continued on Reverse Side]

20. DISTRIBUTION/AVAILABILITY OF ABSTRACT: ☒ UNCLASSIFIED/UNLIMITED ☒ SAME AS RPT. ☒ DTIC USERS	21. ABSTRACT SECURITY CLASSIFICATION: Unclassified
22a. NAME OF RESPONSIBLE INDIVIDUAL: Dr Mitat Birkan	22b. TELEPHONE (Include Area Code): (202) 767-4936 / 22c. OFFICE SYMBOL: AFOSR/NA

DD Form 1473, JUN 86 *Previous editions are obsolete.*

SECURITY CLASSIFICATION OF THIS PAGE
Unclassified

ANNUAL TECHNICAL REPORT

No. UILU-ENG-88-4006

For research supported by
AFOSR Grant No. 87-0169

for period 02/01/87 to 03/15/88

ENERGY CONVERSION MEASUREMENTS IN LASER-SUSTAINED ARGON PLASMAS FOR APPLICATION TO ROCKET PROPULSION

prepared by

Herman Krier(1) and Jyoti Mazumder(1)
David K. Zerkle(2), Ayhan Mertogul(2), and Scott Schwartz(2)

Department of Mechanical and Industrial Engineering
University of Illinois at Urbana-Champaign
1206 West Green Street
Urbana, IL 61801

Work supported by

Air Force Office of Scientific Research
Dr. Mitat Birkan is Program Manager

(1) Co-Principal Investigators
(2) Graduate Research Assistants

APPROVED FOR PUBLIC RELEASE; DISTRIBUTION UNLIMITED

Abstract

Laser propulsion is the production of high specific impulse rocket thrust using a high power laser as a remote energy source. Specific impulses in excess of 1000 seconds are achievable because propellant temperatures are very high and low molecular weight gases can be used. This report focuses on the energy conversion mechanisms of laser-sustained plasmas in flowing argon. The status of AFOSR sponsored experiments to determine thermal efficiency and global absorption is detailed. An improved testing facility has allowed plasma operating conditions never before possible. The results indicate that nearly all of the input laser power can be absorbed by a plasma. Plasmas at elevated gas pressure have been tested, and preliminary results are presented. Optimal operating conditions have yet to be determined for the available laser powers and gas pressures. Further experimentation at very high argon gas velocities (> 20 m/s) must be performed in order to completely characterize plasma behavior.

Fundamental research into the area of enhanced thermal mixing of the extremely high temperature gas with forced cold convection is called for. Multiple plasma testing also is required, as is the testing of low molecular weight gases.

Table of Contents

1. Laser Propulsion Overview

1.1 Introduction

As laser and laser optics technologies become more advanced, laser propulsion promises to be an important means of space propulsion in the decades ahead. With laser propulsion payloads could be transferred within low earth orbit effectively and efficiently. A schematic of how a laser propulsion system might work is shown in Figure 1.1. Remotely beamed laser energy, in this case from a space-based laser, is collected by the systems optics and focused into the rocket's absorption chamber. Here the laser energy is converted into thermal energy of a propellant gas and expanded out a conventional nozzle to produce thrust.

The performance of the proposed laser propulsion system should fill a gap left by the two main current rocket systems, chemical propulsion and electric propulsion. Chemical systems, although capable of high thrust, are limited with respect to specific impulse. Electric systems tend to operate at high specific impulse, but are thrust limited. Figure 1.2 demonstrates this gap graphically, and shows where laser propulsion capabilities fall.

Specific impulse dependence can be shown by the expression

$$I_{sp} \sim (T_o/MW)^{1/2} \qquad (1.1)$$

Where I_{sp} is specific impulse, T_o is the stagnation temperature within the thrust chamber, and MW is the molecular weight of the propellant gas. As shown in the figure, chemical rockets are limited to about 450 seconds of specific impulse. This is due to the combustion chamber temperature being limited by the chemical energy of the propellants, typically below 3500 K, and their high molecular weight, ranging from 12 to 28 kg/kmol. For laser propulsion a low molecular weight propellant can be used (probably hydrogen) and

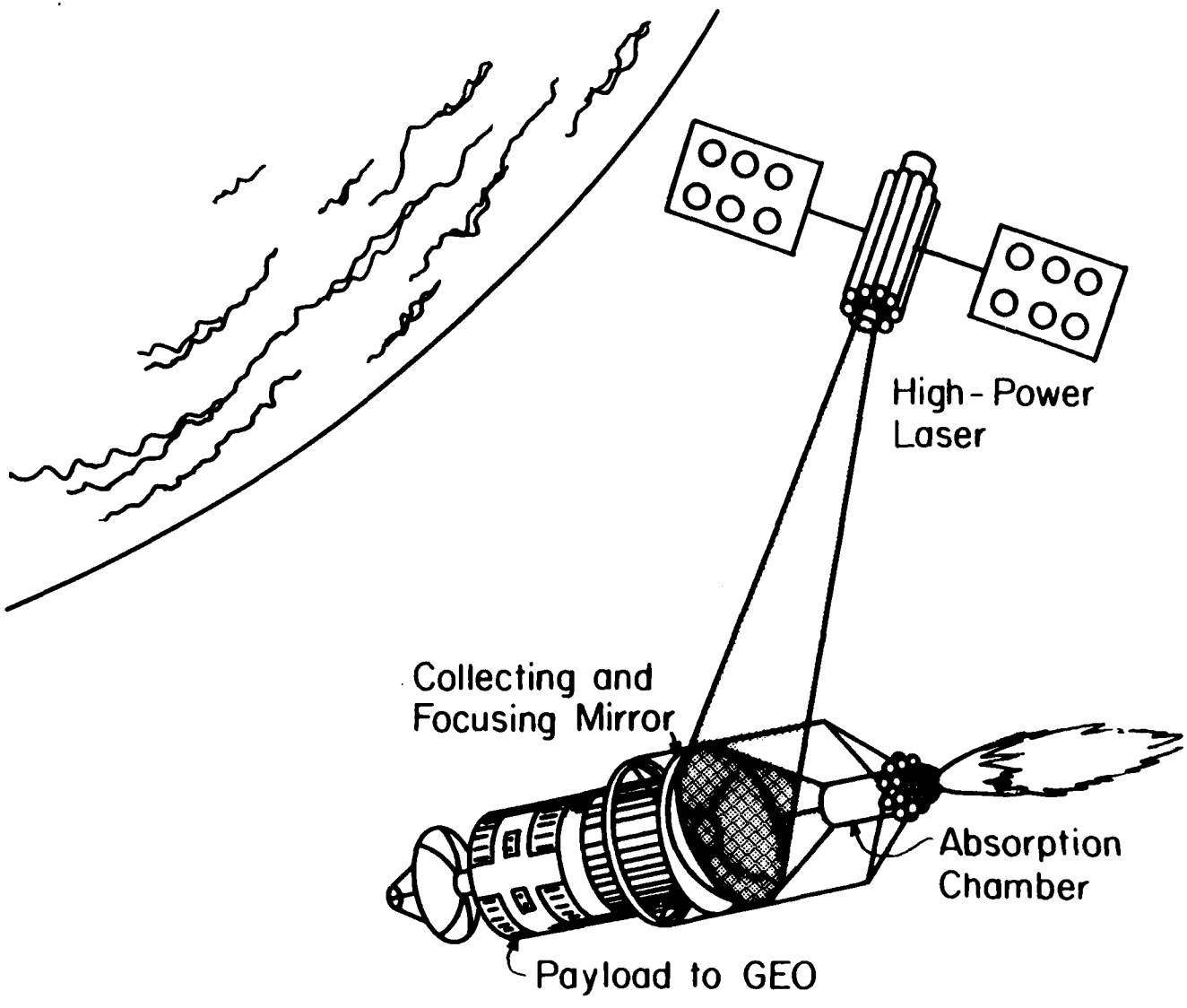

Figure 1.1 Schematic operation of a laser propulsion system used for orbit-raising; Taken from Reference 1.

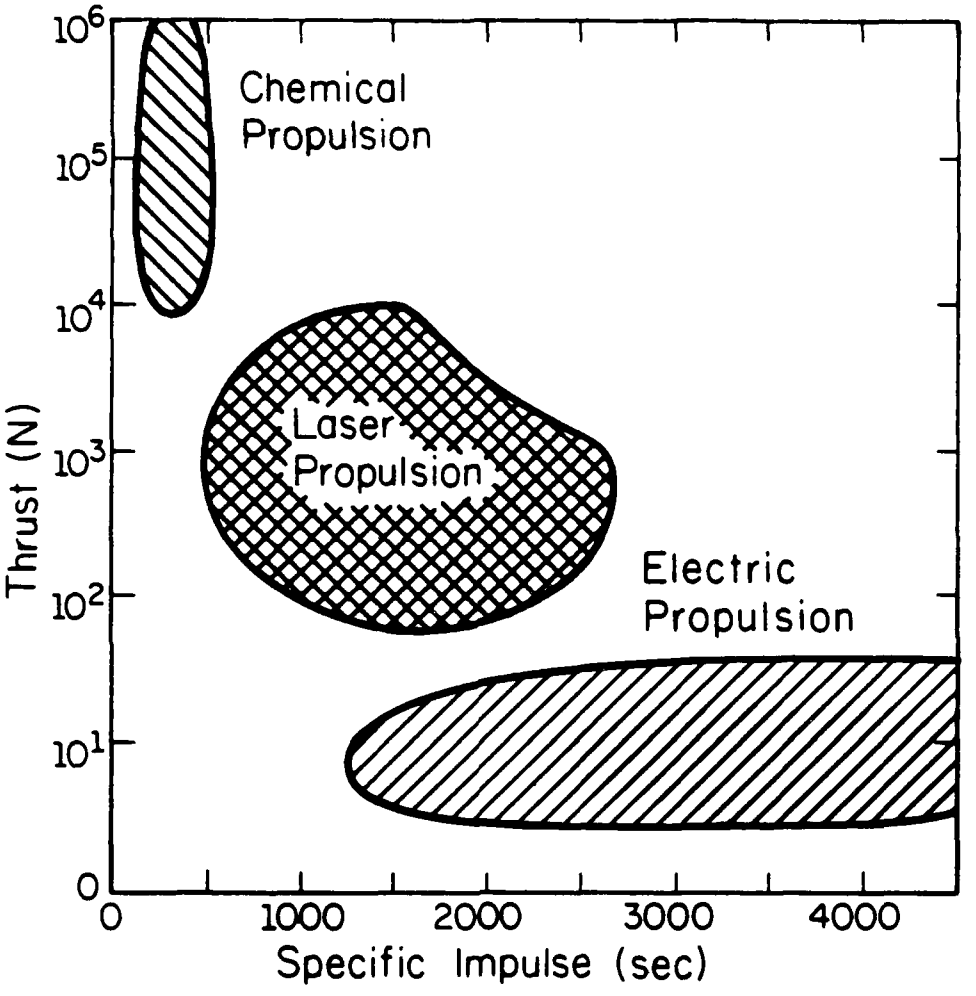

Figure 1.2 Laser propulsion promises to fill the performance gap between high-thrust low-I_{sp} chemical propulsion and low-thrust high-I_{sp} electric propulsion; Taken from Reference 1.

absorption chamber temperatures are not limited by a combustion reaction, but only by material limits of the chamber walls.

Thrust in an electric rocket is limited by the available electric energy on board the space-craft. This electric energy source is usually either a solar energy collection system, or a nuclear reactor. Both of these systems tend to add excessive weight to the craft, and therefore must be kept small thus limiting power. A laser propulsion system, on the other hand, would consist of a remote laser energy source, and therefore be capable of thrust limited only by the available laser power.

Two main concepts have been proposed for converting the beamed laser energy into thermal energy of a propellant gas. These are continuous wave (CW) techniques in which the gas is heated by a continuously operating laser, and repetitively pulsed (RP) techniques, which make use of short rapid-fire bursts of intense laser energy. The CW approach includes both the laser sustained plasma (LSP) and direct laser heating techniques. This work addresses only research done in the area of LSP's, and all discussions will be limited to this CW concept. For discussion and background of other laser propulsion concepts, and the status of current research areas, see References 1, 2, and 3.

1.2 Energy Conversion Mechanisms

The key problem in all laser propulsion schemes is to efficiently convert the input laser energy into thermal energy of the propellant gas. This thermal energy conversion efficiency must be optimized and is the focus of much of this work. It is generally thought that an efficiency of 50% must be realized in order to make laser propulsion feasible, and an efficiency of 90% to make it extremely practical.

A laser sustained plasma appears to be a promising way to achieve the necessary energy conversion needed for laser propulsion. An LSP is a region of high temperature (approaching 20,000 K) ionized gas, and is optically thick to infrared radiation at 10.6 μm

wavelength. As cold propellant gas flows through and around the plasma, it will absorb a certain fraction of the input laser energy at a given set of operating conditions. The rest of the energy is transmitted by the LSP and not utilized in the propulsion system. Of the energy that is absorbed part is immediately radiated to the absorption chamber walls, and can be considered lost to the propulsion system unless some type of regenerative cooling technique is employed. The remainder of the absorbed laser energy is retained by the flowing propellant gas and this high temperature gas can then be expanded through a rocket nozzle to produce thrust. It is this portion of the absorbed laser energy that can be measured by various means and used to calculate thermal energy conversion efficiency. If this retained energy is thought of in terms of a gas enthalpy flux, it can be scaled to input laser power to give a thermal energy conversion fraction.

1.3 Review of Plasma Physics and Laser Optics

1.3.1 Plasma Initiation and Laser Energy Absorption

A plasma will form if sufficient laser power is focused into a gaseous medium (10^9 W/cm^2) or onto the surface of a metal target (10^5 W/cm^2) [4] In this investigation all plasmas are initiated by focusing a 10 kW CW CO_2 laser beam onto a tungsten target which is quickly removed after the plasma is formed. In this process electrons are released due to thermionic emission from the laser heated tungsten surface. These free electrons are available for photon absorption in the presence of an atom or ion. This process is called inverse bremsstrahlung (IB) absorption, and is the dominant mechanism in the maintenance of plasmas within a laser beam focal volume.

The electrons which are excited by IB absorption quickly transfer their energy to surrounding heavy particles through collisional processes. As a result the plasma typically has an absorption coefficient between 10 m^{-1} and 100 m^{-1} at one atmosphere [1], and most of the laser energy is absorbed in the first few centimeters. Total plasma absorption

coefficient is known to increase with pressure, but has a peak in its temperature dependence. The data in Figure 1.3 shows this temperature dependence with increasing absorption coefficient to about 16000 K, then gradually declining at higher temperatures.

1.3.2 Radiation Losses

As mentioned earlier, an LSP will immediately radiate a portion of the absorbed laser energy. Part of this radiated energy is at infrared wavelengths to which the plasma is optically thick and is reabsorbed. Two other radiation components represent energy losses more serious to the thermal energy conversion efficiency reduction. First is free-bound and free-free continuum radiation resulting from a free electron transition to a bound state in an atom, or a free electron transition to another free state in the presence of an atom or ion. This second type of transition is known as bremsstrahlung radiation. The overall continuum radiation has been modeled for plasmas by Oettinger [7], and is found to be a function of temperature and electron number density. Electron number density in turn is an increasing function of gas pressure.

The second radiation loss contribution comes from bound-bound line radiation resulting from electron transitions between bound states of the atom. This type of radiation has been successfully described by Kozlov [8] and is also a function of temperature and pressure. Figure 1.4 shows the temperature dependence of total radiation loss at one atmosphere gas pressure. There is no peak as temperature increases, and an increase in pressure is also known to result in an increase in total radiation loss [1].

1.3.3 Plasma Propagation and Position Equilibrium

A plasma supported in a converging laser beam tends to reside at a position in the beam where plasma propagation velocity is balanced by induced flow velocity. Propagation velocity is a function of the intensity of the laser at a given gas pressure and it

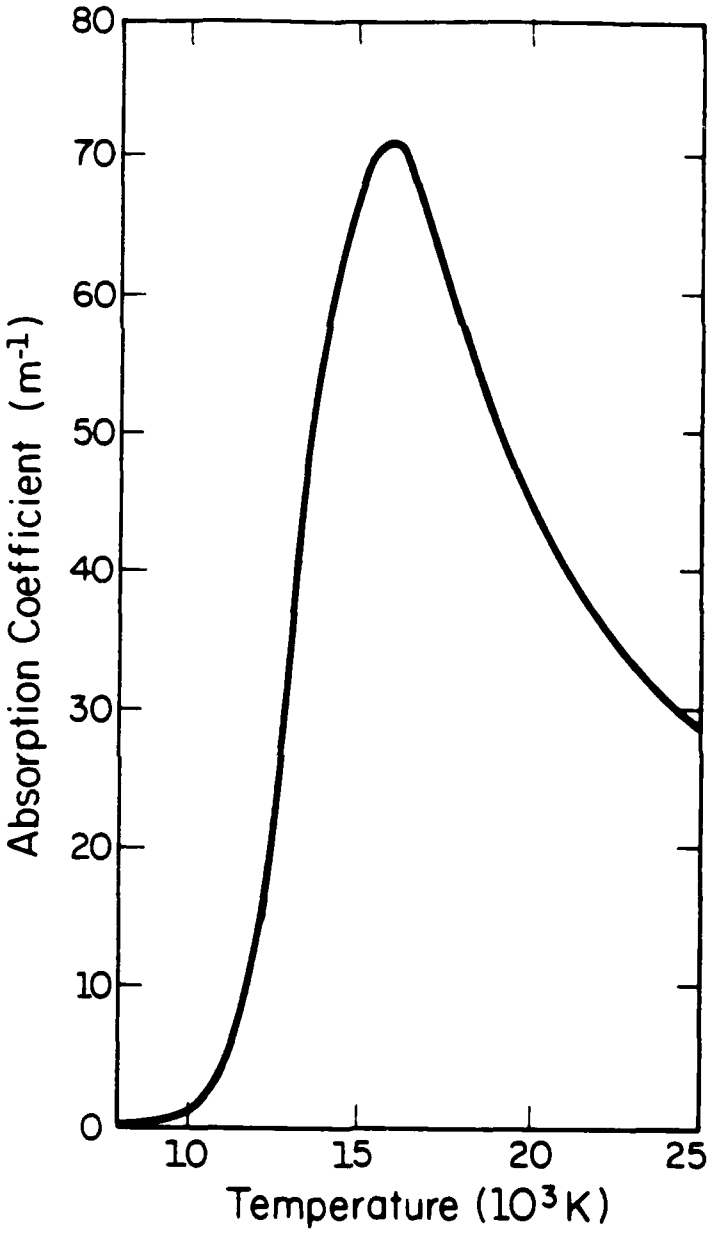

Figure 1.3 Total absorption coefficient of argon at 10.6 μm and atmospheric pressure, calculated using the approach of Wheeler [5] and the correction factors developed by Stallcop [6]; Taken From Ref. 1.

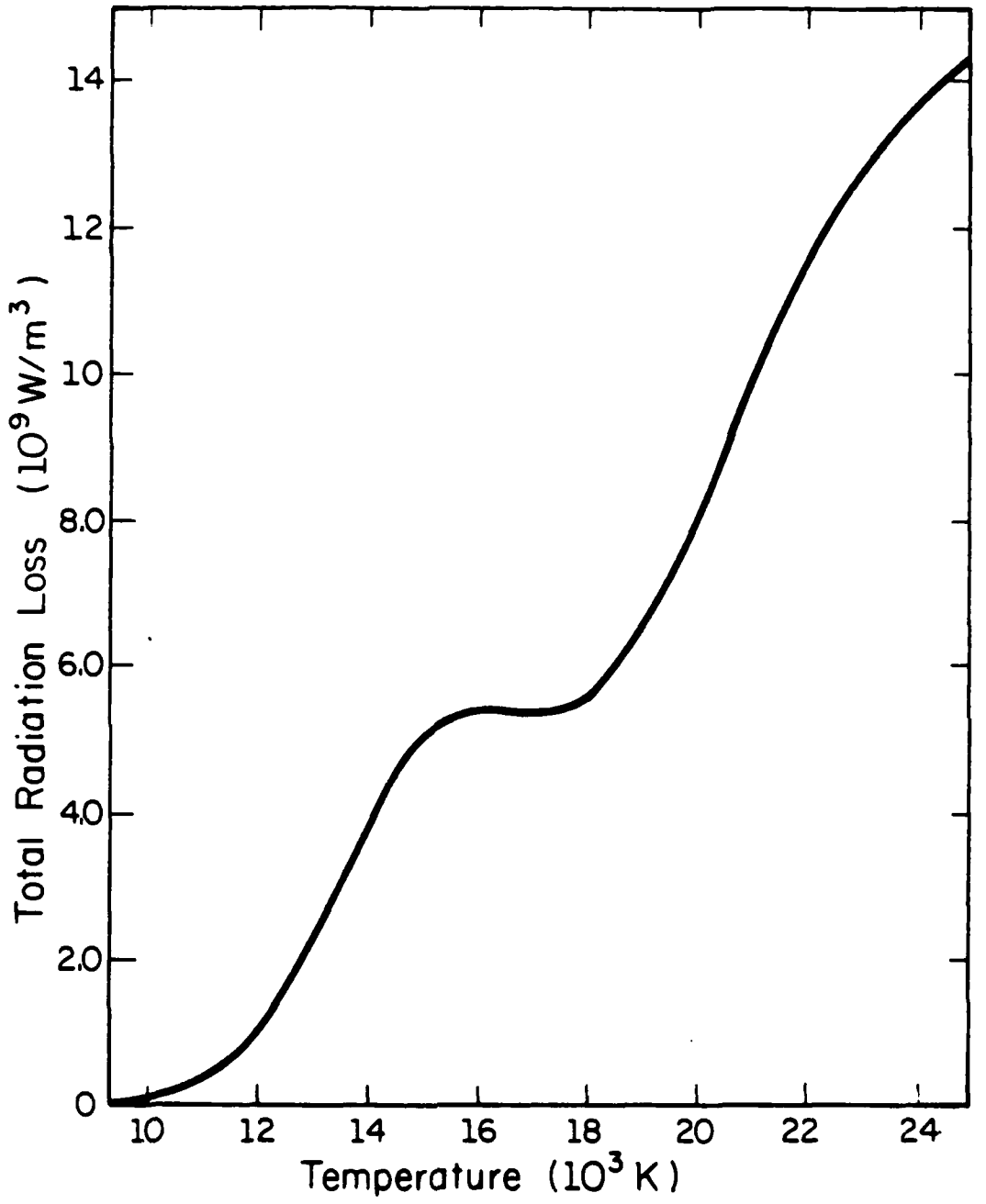

Figure 1.4 Total radiation loss for argon at one atmosphere gas pressure; Taken from Reference 1.

is caused by radiative and conductive heating of gas upstream of the plasma. This heating results in a gas region capable of absorbing laser energy, and the plasma front is shifted upstream into this region. This shifting will continue until the reduced laser intensity of the upstream converging laser beam can no longer produce sufficient heating to overcome the induced gas flow velocity, i.e. cold gas convection.

It is obvious that changing the operating conditions on the LSP will have an effect on the plasma equilibrium position. Total laser power and beam geometry have impact on laser intensity, and changing them will tend to alter plasma propagation velocity. A change in gas pressure can also alter plasma propagation velocity by affecting the absorption coefficient of the plasma front. Within certain limits all these effects can be counteracted by changing the induced flow velocity to achieve the desired plasma position.

For example an increase in laser power will increase the heating rate of gas upstream of the plasma, resulting in an increased plasma propagation velocity and an overall shift upstream. This shift can be offset by increasing the induced flow velocity, forcing the plasma to retreat downstream to a region of higher laser intensity. The reverse of this process can be conceived for a decrease in laser power.

It is theoretically possible to maintain a plasma downstream of the focus in the diverging portion of the beam, but the discussion above shows why these plasmas are unstable and not found in practice. If a plasma in the diverging portion were to experience a small flow disturbance which forced it slightly downstream it would be in a region of relatively lower laser intensity. This lower intensity would cause a decrease in propagation velocity to a level below the nominal flow velocity, causing an even further shift downstream. Thus, the plasma continues to move downstream until there is insufficient laser intensity to support the plasma, and it extinguishes. Similarly, if a small disturbance were to allow the plasma to move upstream into a region of slightly higher laser intensity, its propagation velocity would be increased, and it would continue its upstream propagation

through the focal volume, into a stable region upstream of the focus. Figure 1.5 is a description of the plasma stability phenomenon in the converging and diverging portions of a laser beam.

1.3.4 Laser Optics

Certain optical phenomenon have an effect on the quality of the focal volume and corresponding maximum laser intensity. Theoretically, a parabolic lens or mirror will focus a beam parallel to its optical axis to a single point. As parabolic optical components are very expensive, spherical lenses and mirrors are used in this investigation, and produce spherical aberrations in the focal volume. Spherical aberration becomes more prominent as the radius of curvature of an optical component is reduced. A smaller radius of curvature gives a shorter focal length and therefore a smaller optical f-number, defined as

$$\text{f-number} = f / D \tag{1.2}$$

where f is the focal length and D is the diameter of the incoming laser beam.

Another effect which can be important to the quality of the focus is beam diffraction. Diffraction is inversely proportional to the diameter of the aperture, in this case beam diameter, and not dependent upon focal length. So if a smaller beam diameter is used, focal quality may be limited by diffraction as well as spherical aberration.

Figure 1.6 shows focus spot size dependence on f-number for the 76.2 mm beam diameter used in this investigation. The beam diameter is fixed, so the graph is actually showing dependence on focal length. It should also be noted that actual spot size may be larger due to lens imperfections and manufacturing tolerance limitations. (Appendix A contains information on how Figure 1.6 was produced.) Jeng and Keefer discuss these optical effects and laser beam-LSP interactions in greater detail in Reference 9.

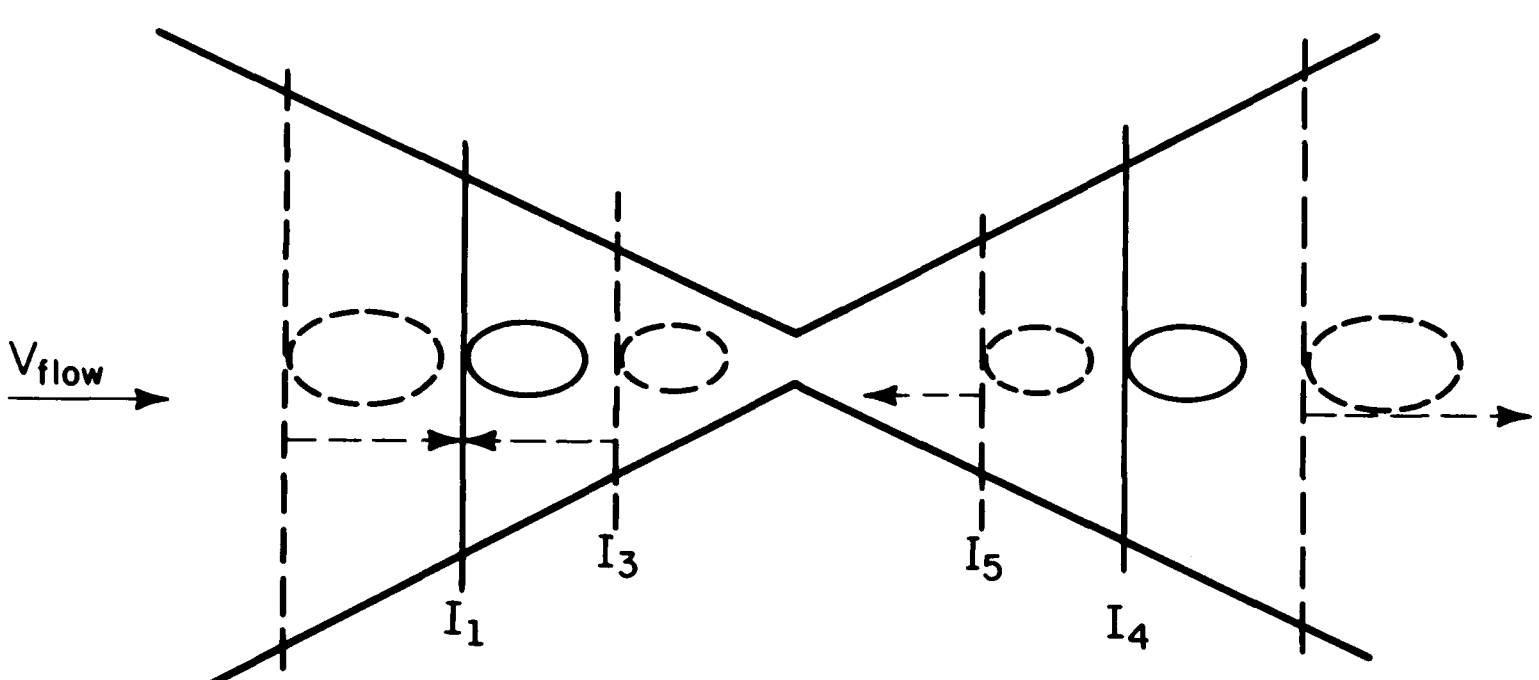

$I_2 < I_1$ so $V_{w_2} < V_{flow}$

$I_3 > I_1$ so $V_{w_3} > V_{flow}$

$I_5 > I_4$ so $V_{w_5} > V_{flow}$

$I_6 < I_4$ so $V_{w_6} < V_{flow}$

Figure 1.5 Plasmas in the converging region of a laser beam are dynamically stable and can adjust to flow variations. Plasmas in the diverging region are unstable and are extinguished by flow variations. In this figure I stands for laser intensity at a certain streamwise location, and V_w stands for plasma propagation velocity at that same location. V_{flow} is the induced gas velocity; Taken from Ref. 1.

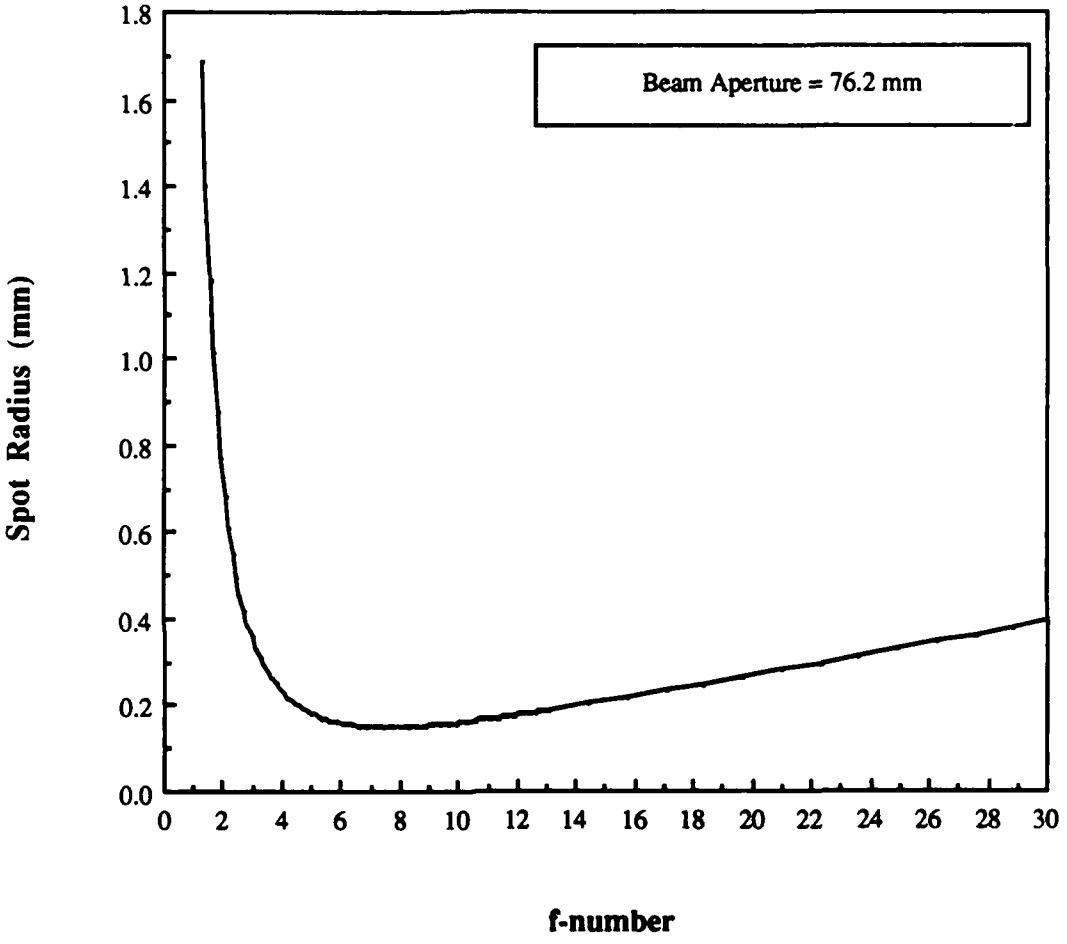

Figure 1.6 Spot size dependence on optical f-number. Dependence on focal length can be inferred because beam diameter (and so diffraction) is fixed.

A final optical effect encountered in this investigation is that of coma produced in the focal volume by an off-axis optical arrangement. Coma is the result of laser beam path length differences resulting in a smeared focal volume. There is a more detailed description of the optics used in this investigation in Chapter 2.

1.4 Past Research Literature Review

Starting in the mid-1970's, laser-plasma interactions have been studied with the concept of laser propulsion in mind. In 1974 Fowler first studied LSP's with a 15 kW CO_2 laser, stabilizing a non-forced flowing air plasma near the focus of a vertical beam [10]. Fowler found that plasmas were stable so long as the optical f-number of the focusing beam did not exceed ten. This is probably due to Fowler's explanation that the plasmas could not adjust quickly enough to fluctuation in flow conditions.

Plasmas in flowing gases have more recently been studied by Keefer [11] and Van Zandt and McCay [12] in a program funded by the AFOSR. Both efforts utilize laser beams focused vertically in pressurized flow vessels. McCay's studies centered on plasmas in flowing hydrogen initiated with a 6 joule, 100 nanosecond, pulsed CO_2 laser and sustained using a 30 kW CW CO_2 laser. Keefer's group has studied low power (<2 kW) plasmas in flowing argon at various pressures, flow velocities, beam geometries, and laser powers.

Both Keefer at the University of Tennessee Space Institute and McCay at NASA Marshall have studied the plasma core using the absolute intensity of continuum radiation measured with a filtered video camera. McCay also filmed plasma initiation sequences with high speed photographs, finding that the pulsed laser creates small localized regions of ionized plasmoids that initially move into the beam, then coalesce into a steady plasma. McCay's experiments at NASA appear to have ended in 1984, apparently due to reliability problems with the 30 kW laser.

Keefer's experiments at UTSI are ongoing, using an advanced version of the spectroscopic video analyzer used earlier. A new CO_2 laser is now being used which is capable of operating with various transverse electromagnetic (TEM) modes, and slightly higher power. Results to date indicate that a plasma will stabilize further from the focus when using higher f-number optics. There is also an observation that absorption fraction decreases at higher f-numbers, and that plasmas were more unstable at higher pressure.

Krier, Mazumder, and co-workers began studies on LSP's in 1983 at the University of Illinois at Urbana-Champaign (UIUC) using a 10 kW CO_2 laser. The UIUC effort utilizes independent techniques for measuring absorption and thermal conversion fractions. A more accurate relative line-to-continuum intensity spectroscopic technique is used to calculate temperature fields in the plasma core. This information is then used to determine fractional absorption and radiation, and hence thermal conversion fraction. In addition calorimetry is used to independently record absorbed power, and thermocouple measurements are used to calculate thermal conversion efficiency from temperature profiles in the absorption chamber exhaust plane. Early results indicated absorption fractions of almost 80% and efficiencies approaching 25% [13].

The spectroscopic and calorimeter absorption data were found to agree fairly well in the UIUC effort, but thermal efficiency calculations agreed only marginally. Uncertainty in spectroscopic radiation loss calculations were cited as the reason for the discrepancies between independent thermal efficiency measurements. In later work by McMillin and co-workers (including the author) [14], thermocouple error was calculated to be also a major contributor to thermal efficiency uncertainty.

In addition to the experimental work done, a quasi-two-dimensional numerical model has been developed by Glumb and Krier [15], which also provides independent theoretical calculation of absorbed power, radiated power, and thermal conversion efficiency. In more recent work, the UIUC group initiated the investigation of multiple plasmas. This work

was presented in Reference 14, and in a terminal paper presented at the AIAA 19th Fluid Dynamics, Plasma Dynamics, and Lasers Conference [16]. Various aspects of multiple plasma operation will be presented here in later chapters.

1.5 Research Objectives

The principle objective of the present investigation is to perform the experiments necessary to characterize and maximize the thermal conversion efficiency of an LSP in flowing argon. As discussed earlier only a portion of the absorbed laser energy will be retained as thermal energy of the flowing argon, the remainder being radiated to the chamber walls. Therefore the fundamental problem is to maximize the overall absorption of laser energy by the plasma while at the same time minimizing the plasma's radiation losses.

Of primary interest in the current research has been the thermocouple measurement of gas temperature for the purpose of calculating thermal energy conversion fraction (Section 3.6). Absorption fraction is determined primarily by the interpretation of calorimeter data (Section 3.5), which provides information on the amount of energy transmitted by the plasma, and thus, energy absorbed. These two results are recorded over a wide range of operating conditions which will hopefully provide adequate plasma characterization. Laser powers up to 7 kW are input to the plasma, and it is exposed to argon flow velocities of over 9 m/s. Although the maximum laser power is 10 kW, it is usually run continuously at a level of only 9 kW. With losses in the optics a typical maximum of 7 kW is achieved. In addition gas pressures ranging from 15 psia to 40 psia are produced in the absorption chamber, and f-numbers from f/2.5 to f/7 are used to help map plasma performance.

Photographs are taken of many of the experimental plasmas, recording relative plasma size, shape, and position with respect to the laser focus for different operating conditions. The intense plasma radiation is filtered before entering the camera lens to prevent

overexposure. This photographic information has been used to help interpret and explain many of the observed phenomenon.

One of the results of the theoretical model of Glumb and Krier [15] was that for certain operating conditions, two small plasmas at equal power may be more efficient than a single large plasma sustained with a power twice that of either smaller plasma, and that higher specific impulse could be obtained. This numerical result was the impetus for the preliminary multiple plasma experiments performed.

2. Experimental Facility

The experimental facility used for the work presented here is much the same as the facility used throughout the UIUC investigation of LSP's. It includes the University's 10 kW CW CO_2 laser, along with much equipment purchased or fabricated specifically for the current investigation. UIUC ME/IE Department Report UILU-ENG-87-4002 [17] contains descriptions of the laser and laser facility, test stand and optics systems, absorption chamber assembly, gas flow system, and data acquisition system used for much of this research. This work will include a brief overview of the above items along with all the changes and additions made to the experimental facility as a whole. The most recent work done with very high flow rates and high pressures involves these changes and additions. Included are a flow straightener on the gas inlet section, a converging quartz section for accelerating the flow, a lens translation stage for positioning of the laser focus, and high precision optical mounts for ease and accuracy of beam alignment.

2.1 Laser

Plasmas are initiated using the University's CW CO_2 infrared laser facility, which is capable of sustained 10.6 μm laser operation at powers up to 10 kW. The laser is an unstable resonator whose output profile resembles that of a TEM_{01}* modeshape, with near-Gaussian energy distribution across the annular cross-section.

The laser facility is shown schematically in Figure 2.1. A technician controls the laser operation from the laser control room, while gas flow and data acquisition systems are operated within the experiment control room. In August 1987, changes were made to the internal laser optics which significantly improved the laser beam quality. Warpage of some water cooled copper mirrors due to internal water pressure was corrected, eliminating much of the beam divergence previously observed. The beam currently is approximately 3 inches

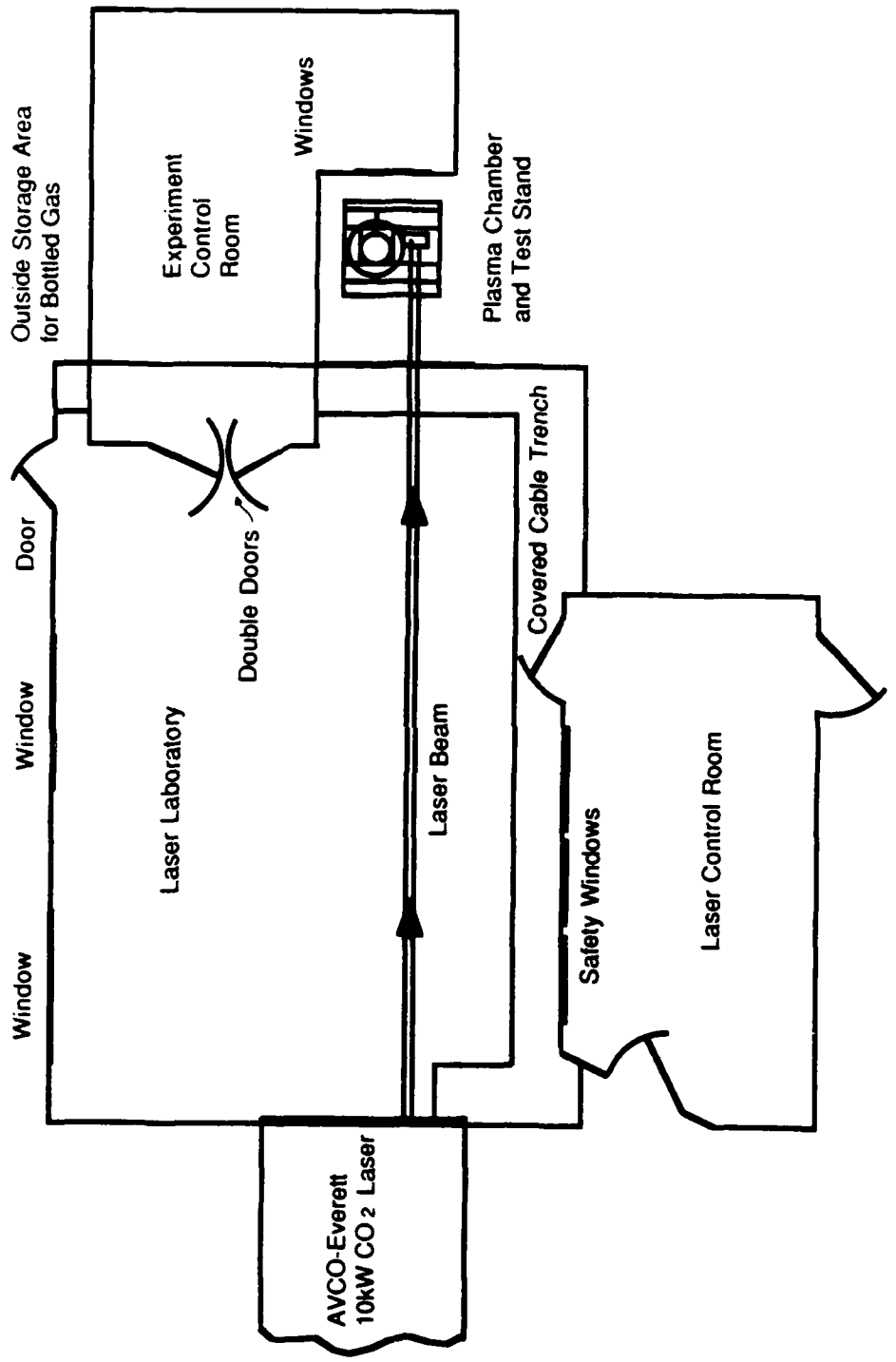

Figure 2.1 Schematic of the Laser Sustained Plasma Experimental Facility; Taken from Reference 14.

in outside diameter, and much of the non-uniformity noted in Reference 14 has been corrected.

2.2 Test Stand and Optical Systems

The test stand is made of steel unistrut framing, and is approximately 3 feet cubed. Figure 2.2 is a drawing showing the complete test stand including the unistrut frame, current optical configuration, translation stage, absorption chamber, and calorimeter. In all optical configurations used the laser beam first strikes the flat mirror in the upper right hand corner of Figure 2.2, and is reflected 90 degrees downward. Two basic optical configurations have been used. The first is off-axis in nature, using a convex-concave mirror arrangement to focus the beam. This configuration was used for the early single plasma experiments, and later for the twin plasma experiments. A schematic of this configuration is shown in Figure 2.3, and a drawing of the split mirror required for the twin plasma application can be seen in Figure 2.4.

The other optical configuration used in this investigation is on-axis, using 5 inch flat copper beam-steering mirrors and a plano-convex sodium chloride lens to focus the beam. This is the configuration shown in Figure 2.2. The on-axis nature of the system eliminates the focal coma associated with the off-axis system described in Reference 14. It also permits a wide range of optical f-numbers to be used by simply changing to lenses of different local lengths. The original design of the on-axis system had all the mirrors and the lens holder mounted and aligned with unistrut fittings. This situation proved to be inadequate due to extreme difficulty in aligning the beam to focus on the tungsten target. The coarseness of the unistrut fittings did not allow for slight adjustments in beam alignment, and proved inconsistent from one day to the next.

The new on-axis system used in taking most of the data presented here consists of precision equipment. The first copper mirror remains (as before), but the two lower flats

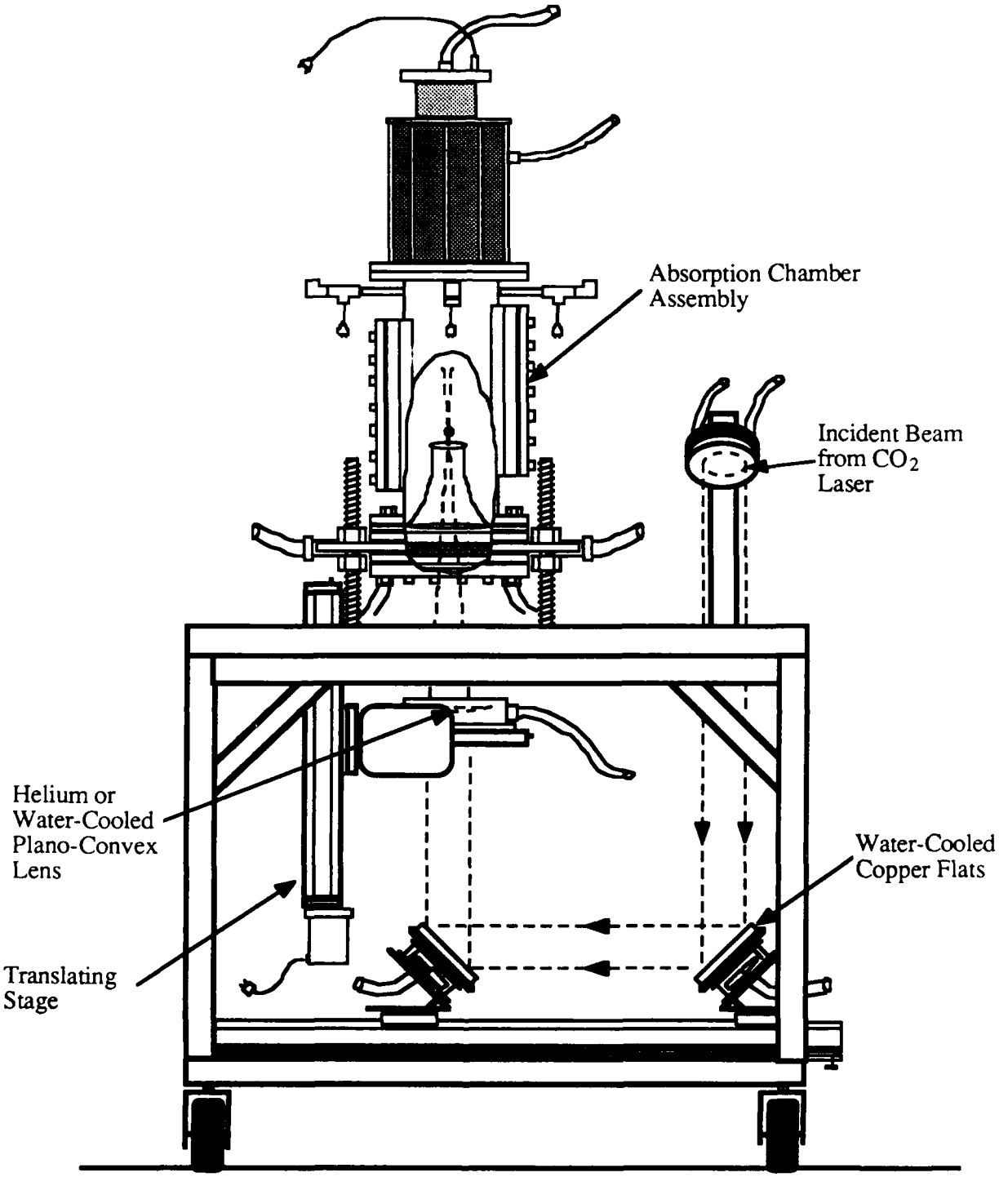

Figure 2.2 Schematic of the test stand used in the study of LSP's. An on-axis optical configuration is shown utilizing precision optical components and a lens translation stage. Taken from Reference 19.

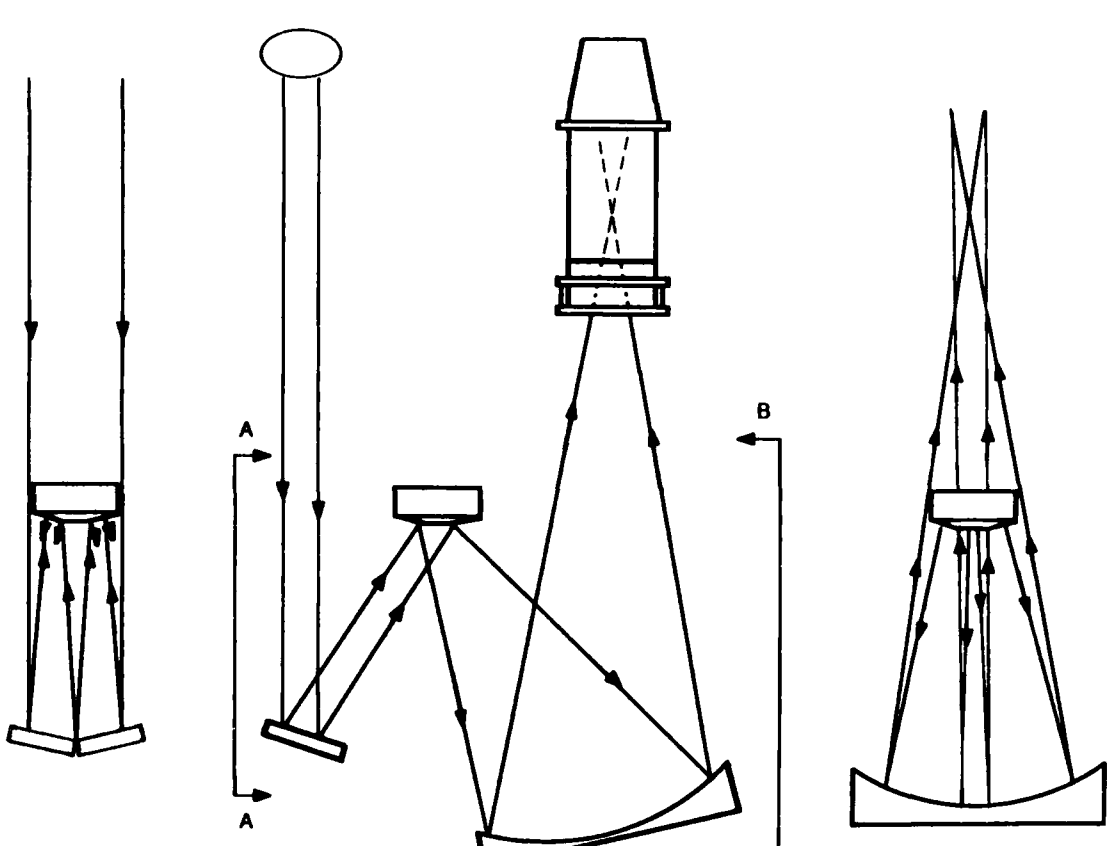

Figure 2.3 Schematic of the off-axis beam steering configuration used to initiate and sustain multiple plasmas. The central view is a composite as seen facing the laser. Views A-A and B-B are side views showing the split mirror arrangement. The apparatus in Figure 2.4 is represented by the mirror in the lower left corner of the composite. The scale of these ray traces has been exaggerated for clarity; Taken from Reference 17.

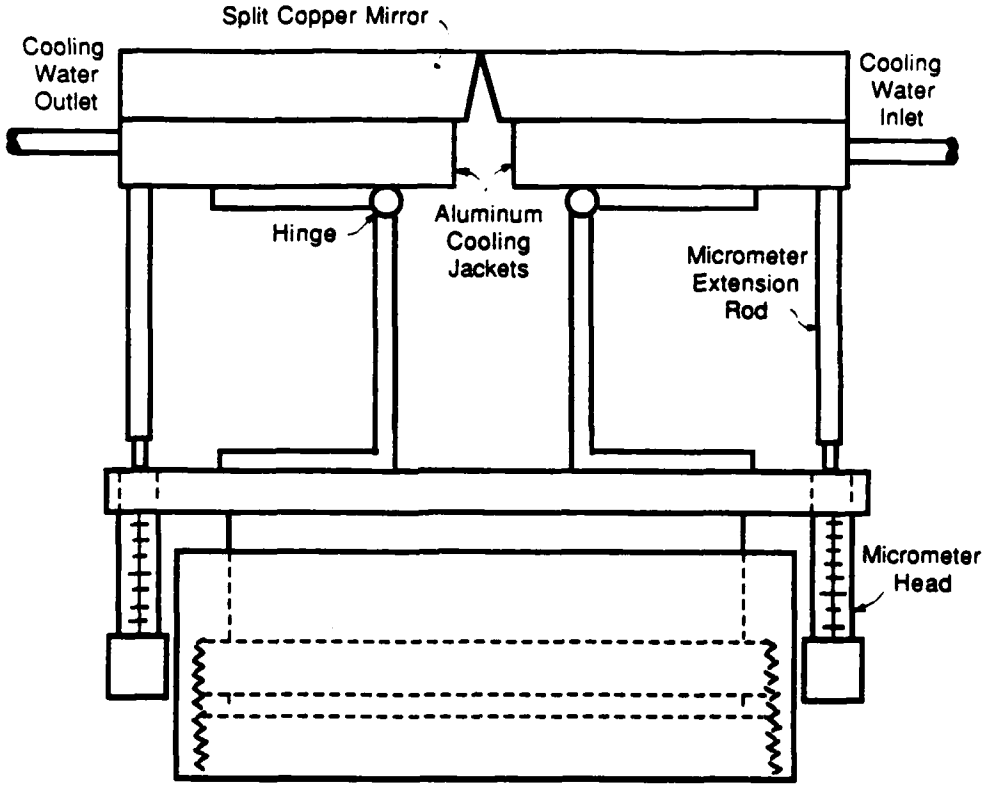

Figure 2.4 Schematic of the split mirror apparatus used in the multiple plasma experiments; Taken from Reference 17.

(pictured in Figure 2.2) now ride on a one meter long optical bench. Each mirror is fixed to an Aerotech 2-axis precision tilt table. The tilt table is then mounted to a Newport 45 degree angle bracket, which provides initial coarse alignment of the beam. The bracket then is bolted to an Oriel universal rail carrier for variable positioning on the optical bench.

For future experiments this on-axis system could be modified to allow for splitting the beam for multiple plasmas. Split mirrors could be used for either or both of the lower beam-steering mirrors. These split mirrors should be mounted on precision tilt tables, ideally with micrometers whose movement could be controlled remotely from the experiment control room.

The current precision beam-steering optics result in a beam aligned very near to vertical. This is important for optimum focusing through the sodium chloride lens. This lens rests in an aluminum lens holder which provides for a flow of helium gas over both faces of the lens. Helium is used because of its high thermal conductivity. Figure 2.5 is a cross-sectional view of the lens holder designed by the author. Helium enters through both outer holes, which are tapped for pipe threads, and flows out over the lens through the annular slots pictured in the figure.

During operation the lens holder rests in a gimbal mounted to a translation stage. The Aerotech gimbal has a 2-axis precision adjustment which allows the lens to be positioned with its optical axis coincident with the centerline of the beam. This is important for a high quality focus and precise focus positioning. In addition, the gimbal was selected so that a new lens holder designed by graduate students Ayhan Mertogul and Scott Schwartz can also be utilized. This new holder is made of aluminum and water-cooled for use with a durable, high strength zinc selenide lens to be used in future experiments. Appendix B contains drawings of the water-cooled lens and window holders for zinc selenide optical components.

The translation stage mentioned earlier is essential for proper vertical positioning of the

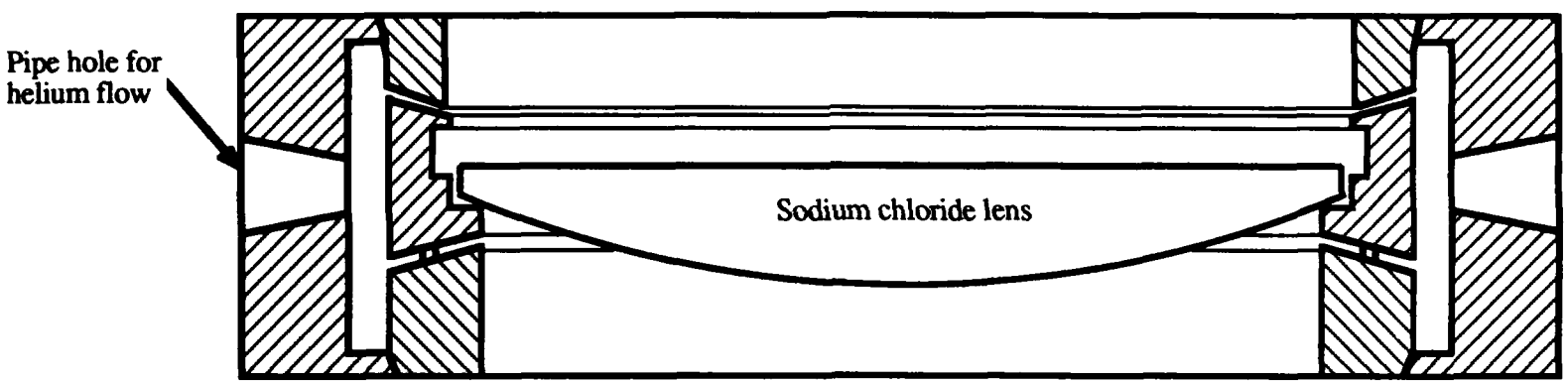

Figure 2.5 Cross-section of the lens holder used to provide helium coolant flow over the sodium chloride focusing lens. Helium is fed in through the pipe holes and flows out of the annular slots onto both faces of the lens.

focus spot for a given set of operating conditions. Particularly, for all experiments in which the quartz converging section is used, the focus must be well above the quartz section in order to focus on the tungsten target for initiation. After the plasma is initiated it must be lowered into the quartz section by lowering the lens with the translation stage.

The translation stage system was designed by Scott Schwartz. The Unislide Series B4000 model B418W25 translating stage has 14 inches of free travel. It is actuated by a Superior stepper motor model MF09-FD08, which is driven by a 24 volt DC power supply controlled by the Fluke measurement and control system. The Fluke system is described later in this chapter.

2.3 Absorption Chamber Assembly

The absorption chamber is shown in Figure 2.6 with its various components labeled. The vertical alignment of the chamber helps to diffuse the effects of the hot buoyant plume produced by the plasma on flow field symmetry.

The significant changes and additions to the chamber assembly have been to the gas inlet section and to the gas temperature diagnostics. Terrence Bender's M.S. thesis [18] contains details on the design and construction of all chamber components. This work will highlight the design aspects important to the experiments and results presented here.

The first change made to the chamber assembly was the addition of a sintered stainless steel flow straightener shown in Figure 2.6. This porous steel piece fits tightly over the inside diameter of the chamber gas inlet section. The twenty-four, 1/8-inch diameter gas inlet holes empty into a narrow plenum groove machined into the outside diameter of the flow straightener. The function of the straightener is to reduce much of the turbulence induced into the flow by the discrete gas inlet jets. The effectiveness of the flow straightener will be assessed in Chapter 4.

A further change made to the chamber was the removal of the axially traversable

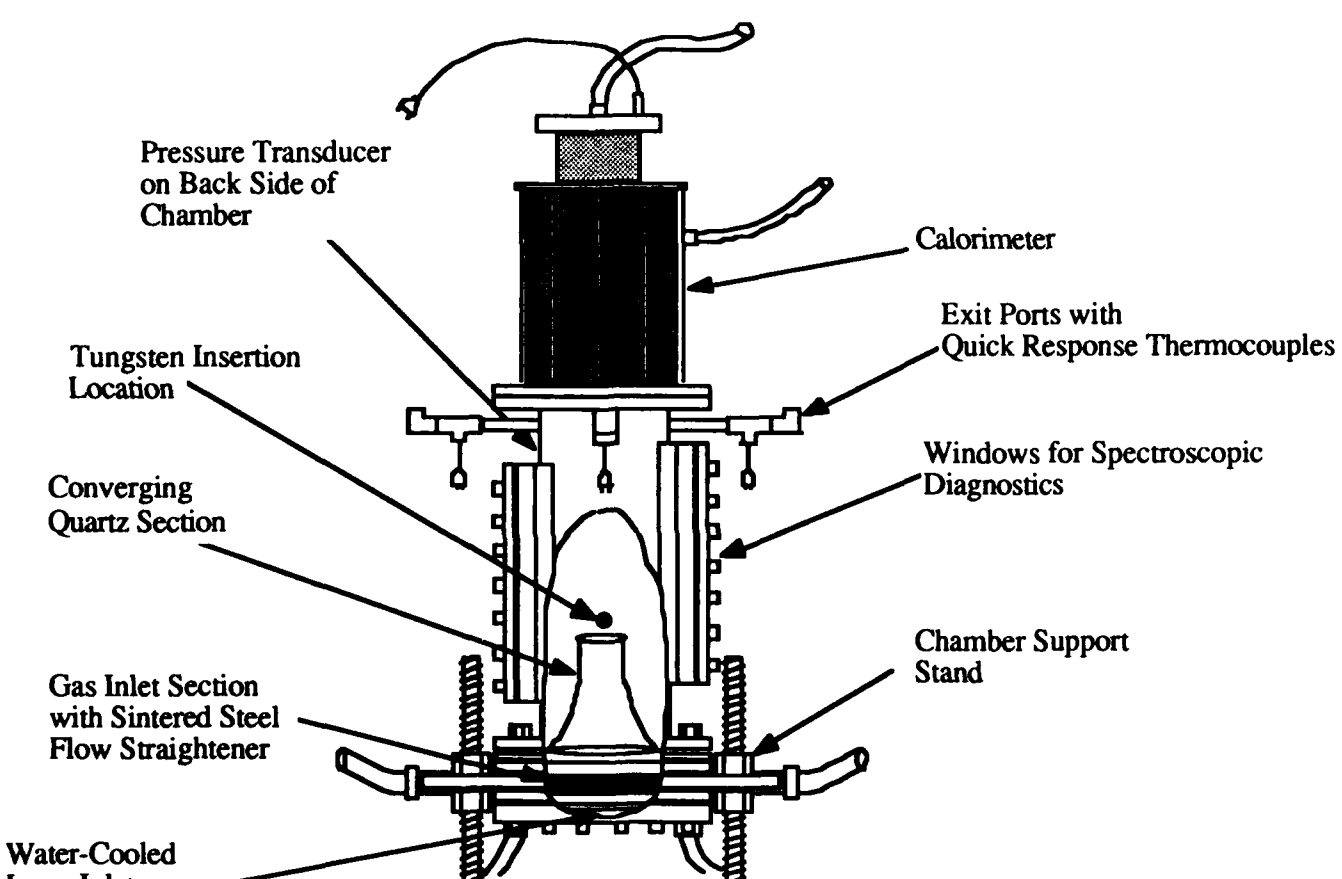

Figure 2.6 Schematic of the absorption chamber used in the study of LSP's. Note the flow straightener and quartz section in the cut-away view; Taken from Reference 19.

thermocouple carriage and stepper-motor driver. This assembly was used for measuring temperature profiles on a chamber radius for the purpose of thermal efficiency measurements. This method of temperature measurement was determined to be inferior to thermocouple measurements in the chamber exhaust ports. Rationale for this determination can be found in Reference 14.

The theoretical model of Glumb and Krier [15] predicted efficiency increases for increasing flow velocity at a given power and f-number. As originally designed the chamber was not capable of stabilizing plasmas at velocities much above 125 cm/s. The causes for this, turbulence and exhaust port compressibility effects, will be discussed further in later chapters. The addition of the flow straightener, and a converging section fabricated from quartz tubing, though, has permitted stable plasmas at almost 16.5 m/s.

There are two quartz tubes that have been used in this investigation. Both are mounted onto 1/8 inch thick stainless steel plates with RTV silicone rubber. Either plate can then be set between the chamber/end receiving flange and the gas inlet mounting flange. This arrangement can be seen in Figure 2.6. The overall length of either tube is approximately 6 inches, with a 2 1/2 - 3 inch straight section in which the plasma is located during an experiment. One tube has an inside diameter of 49 mm, and the other has an inside diameter of 34 mm, in the straight section. For our range of possible argon mass flow rates, the larger tube can provide over 9 m/s velocity at 28.1 g/s and the smaller tube over 19 m/s (at atmospheric pressure).

For all data presented here sodium chloride windows are used at the bottom of the chamber, serving as a laser beam inlet. Sodium chloride has greater than 95 percent transparency to 10.6 μm radiation, but tends to be very weak and prone to cracking under thermal or tensile stress. Polytran windows from Harshaw Chemical are used for high pressure experiments during which regular NaCl windows would fail catastrophically. Polytran is also a sodium chloride compound, produced by hot forging NaCl crystals.

These windows are 1.35 inches thick, and are rated to a pressure of 60 psig with a safety factor of four. In the future zinc selenide windows with an infrared anti-reflection coating will be used. Zinc selenide is much more durable than even Polytran, and does not suffer the caustic effect of water or water vapor that sodium chloride does.

The use of zinc selenide windows and lenses requires that the window and lens holders be water-cooled. As previously mentioned these holders have been designed and fabricated, and are detailed in Appendix B.

The absorption chamber is fitted with side windows as shown in Figure 2.6. They are made of tempered Pyrex and transmit plasma radiation used for spectroscopic analysis of the plasma. These windows are opaque to the laser wavelength and will crack if struck by reflected laser radiation.

The tungsten target used in the plasma initiation process is held into a stainless steel rod mount with a small set screw. The mount screws onto the arm of an air cylinder piston, which is electronically activated from the experiment control room. Thus the target can be inserted and then retracted on command by the experimenter as soon as the plasma has been initiated.

Chamber gas pressure can be monitored and recorded by the Fluke measurement and control system via a pressure transducer. The transducer can measure up to 100 psia with good thermal sensitivity. A pressure relief valve is also mounted to the chamber, limiting the chamber pressure to 5 atmospheres to protect the windows and transducer.

Chamber wall temperature can also be monitored and recorded by the Fluke system. Presently the temperature is monitored only at one point, at approximately plasma height. A type T thermocouple has been embedded into the chamber wall, giving a very accurate measure of temperature. Originally this was supposed to give an estimate of radiation heat loading of the chamber walls, but due to the non-isothermal nature of the chamber this proved to be a very inexact measure. More recently the chamber wall temperature has been

used to help understand convection losses from the hot downstream gas as operating conditions are changed [17].

All gas temperature measurements used to calculate thermal conversion efficiency are made with millisecond response time type K thermocouples. There is one thermocouple in a gas inlet port to measure inlet gas enthalpy flux, and one thermocouple in each of the four exhaust ports to measure the gas enthalpy after having passed through and around the plasma. It is the difference in these enthalpy fluxes that determines the thermal energy conversion fraction. To help reduce radiation error, each thermocouple junction is shielded from the port walls. In addition, placement in the ports and not out in the chamber virtually eliminates direct plasma or laser radiation heating of the thermocouple junction, thus reducing overall error. However, as discussed in Chapter 4 the further downstream of the plasma the gas temperature is measured, the more significant convection heat losses become.

In order to increase the gas pressure in the chamber, a valve has been installed which connects all four exhaust ports. As shown in Figure 2.7, 1/2 inch copper tubes extend from each port to be joined with pipe/tube fittings, forcing the exhaust gases into one 1/2 inch polyflow tube. The pressure control valve is located at the end of the polyflow tube near an opening in the ceiling of the experiment control room. This allows manipulation of the pressure during an experiment, yet still directs the exhaust gas outside of the control room. One experimenter must read pressure from the Fluke system monitor while another reaches up to manipulate the valve, making it somewhat difficult to achieve precisely the desired pressure. In the future a valve with much better resolution should be used so that more accurate and repeatable pressures can be achieved.

Another problem with the high pressure system is that currently, no chamber gas pressure between one atmosphere and two atmospheres can be achieved due to friction in the exhaust tubing. The gas pressure is approximately one atmosphere when the exhaust

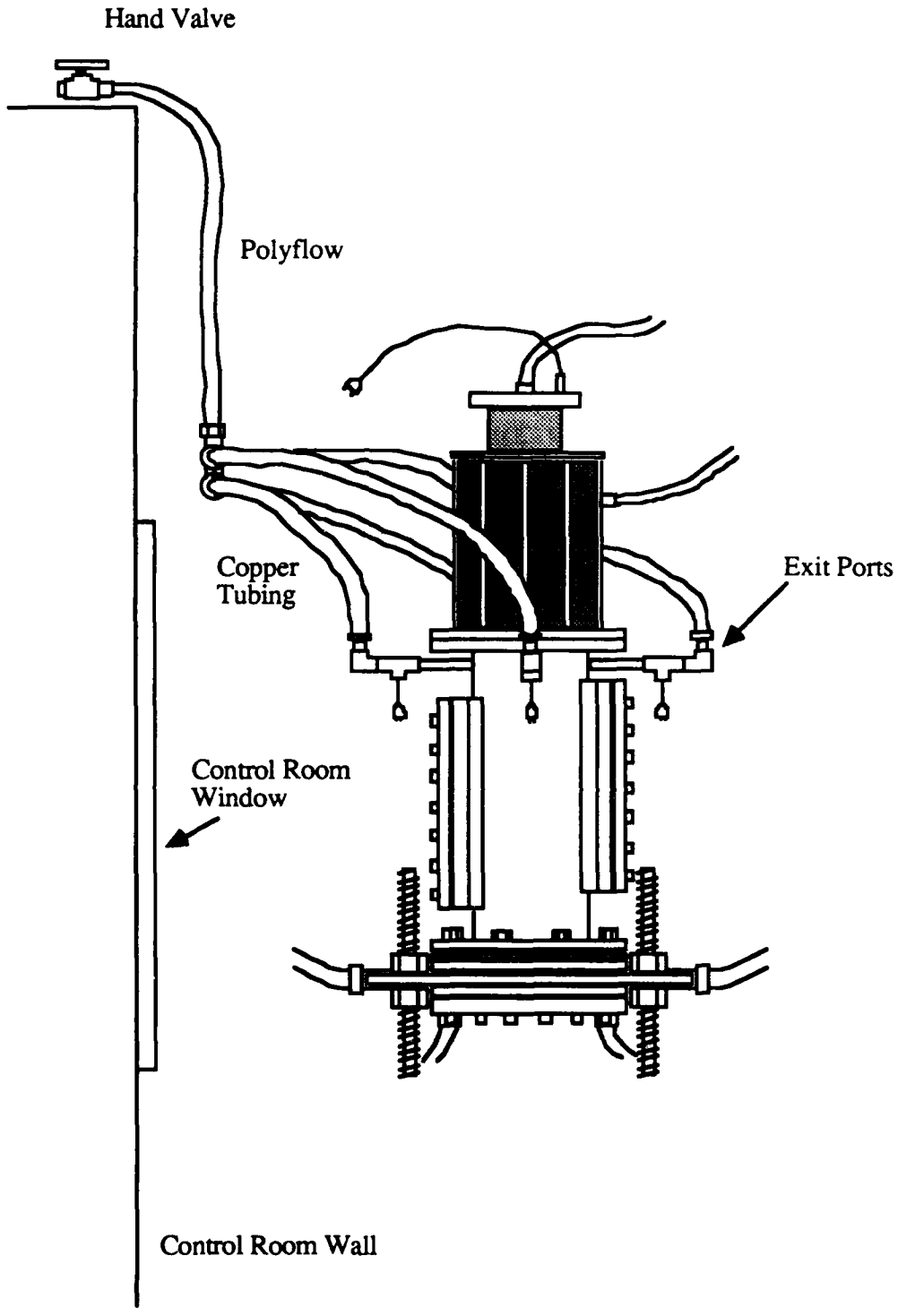

Figure 2.7 Schematic of system used to control chamber gas pressure.

ports discharge directly into the room, but jumps to two atmospheres when the copper and polyflow tubing system is installed with the control valve in the fully open position. For future high pressure experiments a system should be designed which allows virtually all pressures above one atmosphere with good accuracy and precision.

The calorimeter used to collect absorption data can bolted directly to the top of the chamber, as shown in Figure 2.6, or a sodium chloride window can be sandwiched between the chamber and calorimeter as shown in Figure 2.8. Details on calorimeter operation can be found in Reference 17. In this investigation the NaCl window has a twofold purpose. Most importantly it provides a barrier to keep the hot plasma exhaust gases from entering the calorimeter and being convectively cooled before flowing past the exhaust port thermocouples. Also, it helps to decouple the laser heating of the calorimeter, and the gas heating. The overall effect of the hot gases entering the calorimeter is that thermal efficiency appears low because the gas is being cooled, while absorption fraction also appears low due to the gas heating of the calorimeter.

2.4 Gas Flow System

All the experiments undertaken in the current investigation utilize the high mass flow system described in Reference 17. With the exception of the steel flow straightener added to the gas inlet section of the absorption chamber, all components are unchanged from the previous work. The low mass flow system is still intact, but unused with the experiments concentrating on high velocity and pressure.

2.5 Data Acquisition System

As mentioned previously a Fluke measurement and control system is used when running many of the experiments in this study. All thermocouple, chamber pressure, calorimeter, and translation stage position data are scanned approximately every 1.5

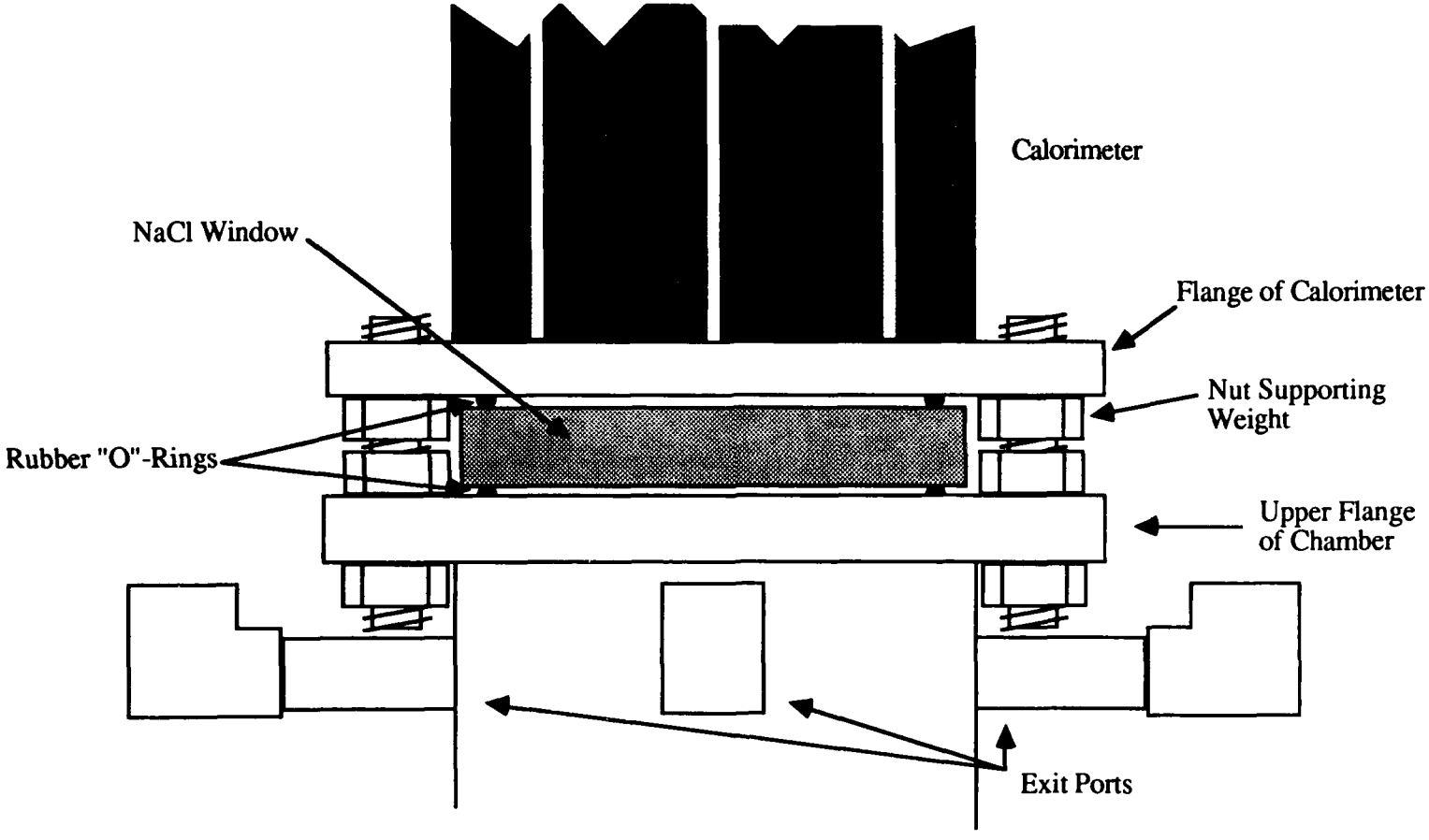

Figure 2.8 Schematic of sodium chloride window sandwiched between the chamber and calorimeter. This method relieves the weight of the calorimeter from the window; Taken from Ref. 19.

seconds. Much of this data appears on the screen of the computer, providing immediate experimental feedback. At the completion of an experiment the data can be stored on a floppy disk and later uploaded to a Cyber 175 mainframe computer for reduction. A concise description of the operational commands and capabilities of this system are included in Reference 18. The original software in Reference 18 was modified by Brian McMillin to include additional data taking capabilities currently being used. McMillin's modified version is described in Reference 14 and a listing of it can be found in a notebook entitled "PIFC Revised Source Code Listings" on file in 212 MEL, UIUC. Further modifications were undertaken by Scott Schwartz and include the ability to monitor all four exhaust port thermocouples, calorimeter output, and translation stage position. Schwartz's modifications are described in better detail in Reference 19.

Schwartz has recently designed a system utilizing a Macintosh personal computer and hard disk for data reduction and storage. This system will eliminate the lengthy data uploading process, and enable the reduced data to be plotted directly using Macintosh software.

3. Experimental Technique and Data Analysis

As stated earlier the current investigation has centered on the use of thermocouple and calorimeter measurements. Also, photographs taken with a filtered 35 mm camera are used in conjunction with these conventional means to analyze experiments.

Emission spectroscopy has been the most widely used method for examining LSP's, and a relative line-to-continuum technique has been used here at the UIUC. The application of independent experimental techniques is unique to the effort here, but in this work the spectroscopic results will be limited to the discussion of plasma symmetry. References 1 and 4 contain a thorough examination of the UIUC spectroscopic effort.

This chapter includes discussion of the conventional thermocouple and calorimetric methods of data collection, and the methods used to analyze the data. Laser power measurement techniques and a review of beam quality will be presented, along with an evaluation of inlet flow turbulence and consequent flow straightening. Problems with high mass flow rate experiments will be discussed, including compressible flow in the inlet and exhaust ports, and chamber gas pressure build up. In addition the technique used for calculating thermal energy conversion efficiency is detailed.

3.1 Laser Power and Beam Quality

Laser power input to the plasma is a very important parameter, as is the quality of the laser beam configuration. In order to make accurate evaluations of thermal energy conversion efficiency, one must know the original amount of energy under consideration. This requires that measurements be made which permit the calibration of energy leaving the laser. Additional measurements are made at several points in the optical path which help to determine losses, i.e. partial absorption or back reflection of the laser beam at each optical component. Thus laser power delivered to the plasma is determined with a fair amount of

accuracy.

3.1.1 Laser Power Measurement

All laser power measurements made to date have been with a Series 25 Laser Power Probe Manufactured by Optical Engineering, Inc. Operation of this probe is detailed in Reference 14. It's accuracy and repeatability are specified to be within 5% and within 2%, respectively. The first in a series of measurements at a given power is usually not repeatable, and not used in evaluating laser power. The reason for this initial measurement inaccuracy is not known.

The on-axis optical system described earlier results in a power loss of about 27%. There is variation in power loss when using different windows or lenses, and these must be considered individually. In addition, as power losses are determined when all windows, lenses, and mirrors are at room temperature, some underprediction of losses is to be considered. This is because window and lens losses have been found to increase slightly with temperature [14], and these components tend to heat up during use.

It should be noted that power losses presented here are only approximate and representative. In practice the power input to the plasma is calibrated for each pre-optics laser power. Calibration charts used in this investigation can be found in the research data book located in room 212 MEL.

3.1.2 Laser Beam Quality

In the past and as noted in Reference 14, the laser beam, due to its own optics, tends to be slightly divergent and circumferentially non-uniform. This led to significant losses in the test stand optics because the divergent beam was not being fully captured at each mirror. Also, the beam had become too large in diameter to fit through the lens holder aperture of 3.62 inches.

At the request of the researchers involved in this investigation, the Materials Engineering Research Laboratory (MERL) Laser Staff attempted in late 1987 to improve the laser beam quality. In the course of their work two mirror alignments were performed. In the first, external adjustments were made which improved the beam significantly. In the second alignment, the water-cooled copper mirrors were fine tuned to compensate for warpage due to internal water pressure. The results of beam profile burns in plexiglas (a method described by McMillin [14]) showed that the beam was no longer as divergent, and was much more uniform circumferentially. The beam is currently being sufficiently captured by all mirrors and does not interfere with the lens holder at all.

It is thought that beam uniformity may have an effect on plasma stability, and this is demonstrated in the next section. Raw spectroscopic emission data was taken before and after the MERL staff last worked on the laser beam quality. These tests led to the conclusion that the plasma was much more symmetric following the beam fix. A more symmetric plasma gives evidence for the more uniform laser beam.

3.2 Plasma Stabilization

One of the primary concerns with LSP's used for laser propulsion is the value of the maximum flow velocity at which a plasma is stable at a given power. (This maximum flow velocity is called the blowout velocity.) Characterizing blowout velocity is considered an important step toward designing an actual rocket thruster because the mass flows, fixed by laser power and specific impulse, will determine the gas velocity inside the absorption chamber.

In the study of blowout one looks for the plasma's equilibrium position to be shifted downstream by the flow to the point where the plasma front is at the laser focus. Theoretically, any further increase in flow would force the plasma entirely into the diverging portion of the laser beam. As discussed in Chapter 1 the plasma is unstable in

this portion and will extinguish.

In earlier work the blowout phenomenon was never observed quite as described above. In all cases the plasma would begin to bounce (oscillate vertically) as flow velocity was increased. It eventually extinguished before the plasma front ever reached the focus, and therefore at much lower velocities than expected. The two major reasons for this were effects due to inlet gas turbulence and laser beam asymmetry.

3.2.1 Laser Beam Asymmetry

As just mentioned in section 3.1 laser beam symmetry has an effect on plasma stability. Figure 3.1 is a graph showing the velocities at which the plasmas of various powers extinguished. The three highest curves show the effect of the two beam alignments performed by the MERL staff. As the figure shows, a more symmetric beam allows a significant increase in the velocity at which a given power plasma will extinguish. These measurements were taken at one atmosphere gas pressure.

This result shows that what has previously been thought of as plasma blowout was really a symptom of poor quality laser capabilities. Although much improved, the current beam symmetry is not perfect. It is obvious that further improvements to the beam quality would most likely improve plasma stability. The beam alignment process is very time consuming (about two weeks) and it is impractical to perform with great regularity. At the least the alignment should be performed once a year, and more often if significant asymmetries develop sooner.

3.2.2 Inlet Gas Turbulence

Another factor which has proved to be very important to plasma stability has been inlet gas turbulence. As originally designed, the inlet gas section consists of twenty-four 1/8 inch diameter holes directed radially inward. Some of these holes are pointing

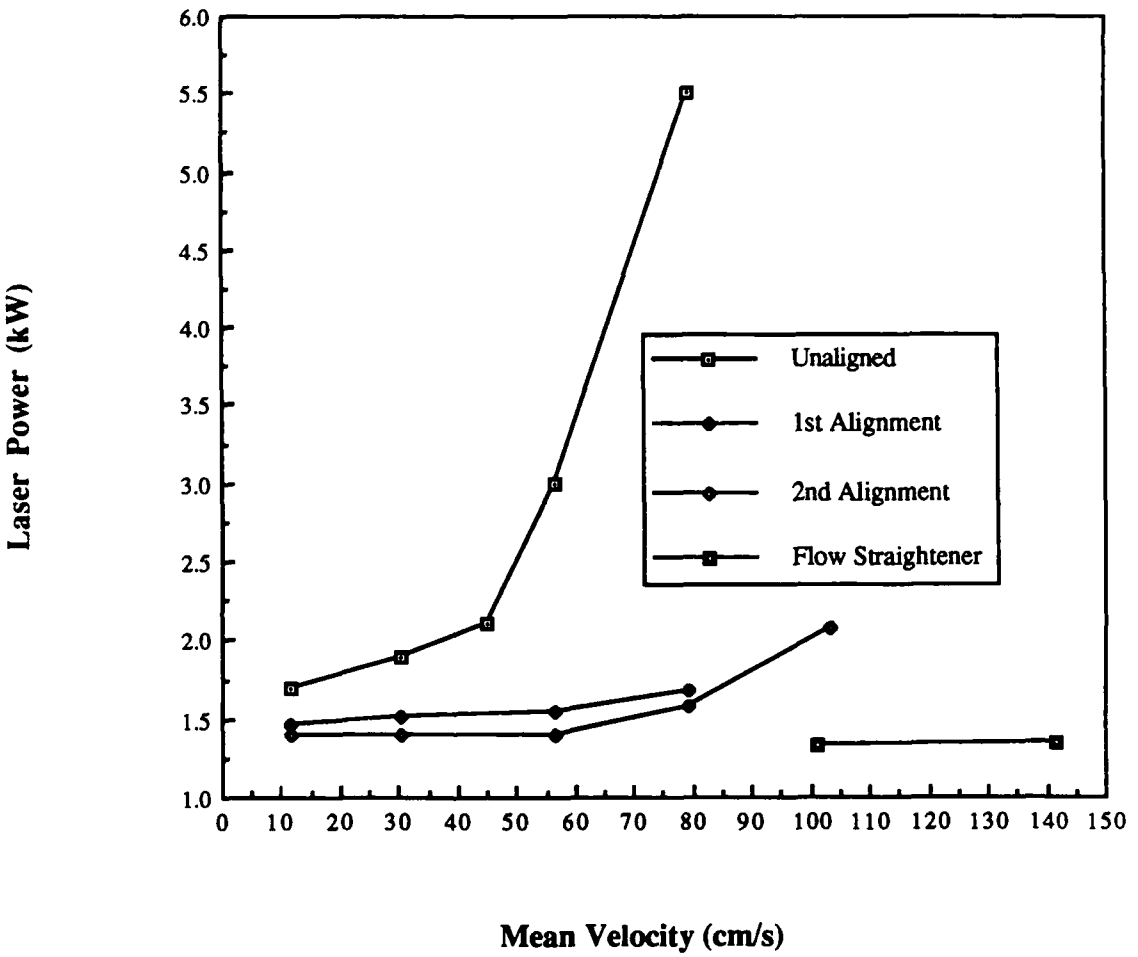

Figure 3.1 Mean argon gas velocity at which a plasma extinguishes. The different curves show the effects of beam alignment and flow straightening.

downward to provide some cooling flow on the laser inlet window, and some are pointing upward. The turbulent nature of circular jet flow , coupled with the inlet hole arrangement leads to a noisy chamber flow condition. A flow visualization technique has shown that the gas typically spirals counterclockwise at about 3 Hz exhibiting large turbulent eddies [18].

To correct this condition, a sintered stainless steel flow straightener was inserted over the existing inlet holes. This straightener, described in Chapter 2, dampens the flow disturbances considerably, and Figure 3.1 presents data showing the effect on plasma stability. The two points representing a curve for straightened flow show a dramatic increase in the velocity at which two plasmas very close in power extinguished. To test plasmas at higher powers would require putting too much mass flow through the chamber to maintain atmospheric pressure, but the trend is obvious. The improvements in beam quality and inlet flow straightness opened the doors for experimenting with stable plasmas at velocities much higher than was originally thought possible with our test facility. The problems with pressure build up and compressible inlet and exhaust flows due to high mass flow rates are dealt with in following sections, and the results of high velocity plasma experiments are presented in Chapter 4.

3.3 High Gas Flow Rate Considerations

With the improvement of beam quality and the addition of a flow straightener stabilizing plasmas at high velocities (above 1.5 m/s) became possible. With the absorption chamber as originally designed, however, very large amounts of argon gas must be forced through the system to obtain elevated velocities (over 40 g/s for 2 m/s). This condition brought about two new problems in experimental procedure and data analysis: 1) compressible flow and 2) pressure build up.

As designed, the inlet and exhaust ports (each 1/2 inch in diameter) began to accelerate the flow into the compressible regime at some elevated mass flows. This presents a

problem because it is impossible to directly measure exact static temperature with a stationary device in a moving fluid [20]. If static temperature, T, were known, stagnation temperature, T_o, could be found by the relation

$$T_o = T(1+((\gamma-1)/2)M^2) \tag{3.1}$$

if, γ , the ratio of specific heats of argon, and, M, the Mach number are both known. Stagnation temperature is the quantity of interest for an enthalpy calculation, and could be estimated, rather than calculated, in a compressible flow with the use of a probe specially designed for recovering this quantity [20]. The easiest way, however, to obtain an accurate estimate for stagnation temperature is to modify the conditions such that the gas velocity in the ports is low enough to be considered incompressible. In this instance, static and stagnation temperature are virtually equivalent and can be measured quite accurately with a shielded fast response thermocouple.

Mach number can be determined by the following relation

$$\dot{m}(RT_o)^{1/2}/P_oA = M(\gamma)^{1/2}(1+((\gamma-1)/2)M^2)^{-(\gamma+1)/2(\gamma-1)} \tag{3.2}$$

if stagnation pressure, P_o, stagnation temperature, T_o, and mass flow rate, $\dot{m}$, are known. In the incompressible flow regime (Mach number <0.3) the stagnation quantities can be taken as those measured with the pressure transducer and thermocouples in the chamber assembly. The above relation predicts a Mach number of 0.3 in the inlet ports at a mass flow rate of about 41 g/s for most cases.

As a 41 g/s mass flow rate only produces 2 m/s flow velocity in the 5 inch diameter chamber, the converging section discussed in Chapter 2 was added to accelerate the chamber flow to desired velocities at mass flow rates which are acceptably low. The

resultant incompressible flow allows for reliable gas temperature measurements in all cases.

The other problem with high mass flow rates is pressure build up in the chamber. The curve in Figure 3.2 shows how the chamber pressure increases with mass flow due to the restrictions at the exhaust ports. 41 g/s mass flow rate produces only about 108 kPa gas pressure in the chamber, which corresponds to 1.07 atmospheres. It is important to be able to keep chamber pressure constant throughout a series of experiments for analysis purposes. As pressure goes up so does density, which in turn has an effect on gas absorptivity at 10.6 μm. So if pressure is not constant with mass flow, a series of experiments intended to examine the effects of varying mass flux (kg/sm^2) only (i.e. velocity only) are impossible. The effect of a pressure increase is permanently coupled to this type of experimental series. No available analysis could determine if experimental results are due to pressure changes or mass flux changes.

The converging section increases the mass flux without having to increase the mass flow rate (g/s). Two different sections can be used presently, each raising mass flux by a different constant factor over the original design. One section converges to 49 mm giving an increase of almost seven times the flow velocity from the original 5 inch diameter chamber. The other section is 34 mm in diameter, which corresponds to a velocity increase of almost 14 times. The arrangement of these sections (made out of quartz for this high temperature application) can be seen in Figure 2.6.

The addition of the interchangeable converging sections to the flow chamber has enabled several problems to be successfully overcome. However, as a result of this particular advancement another problem has arisen. Due to the significant change in the way the argon gas flows through the system with a quartz section in place, changes have come about in the way energy gained from the laser beam is distributed in, and lost by, the gas. Those results and their impact will be discussed in Chapter 4.

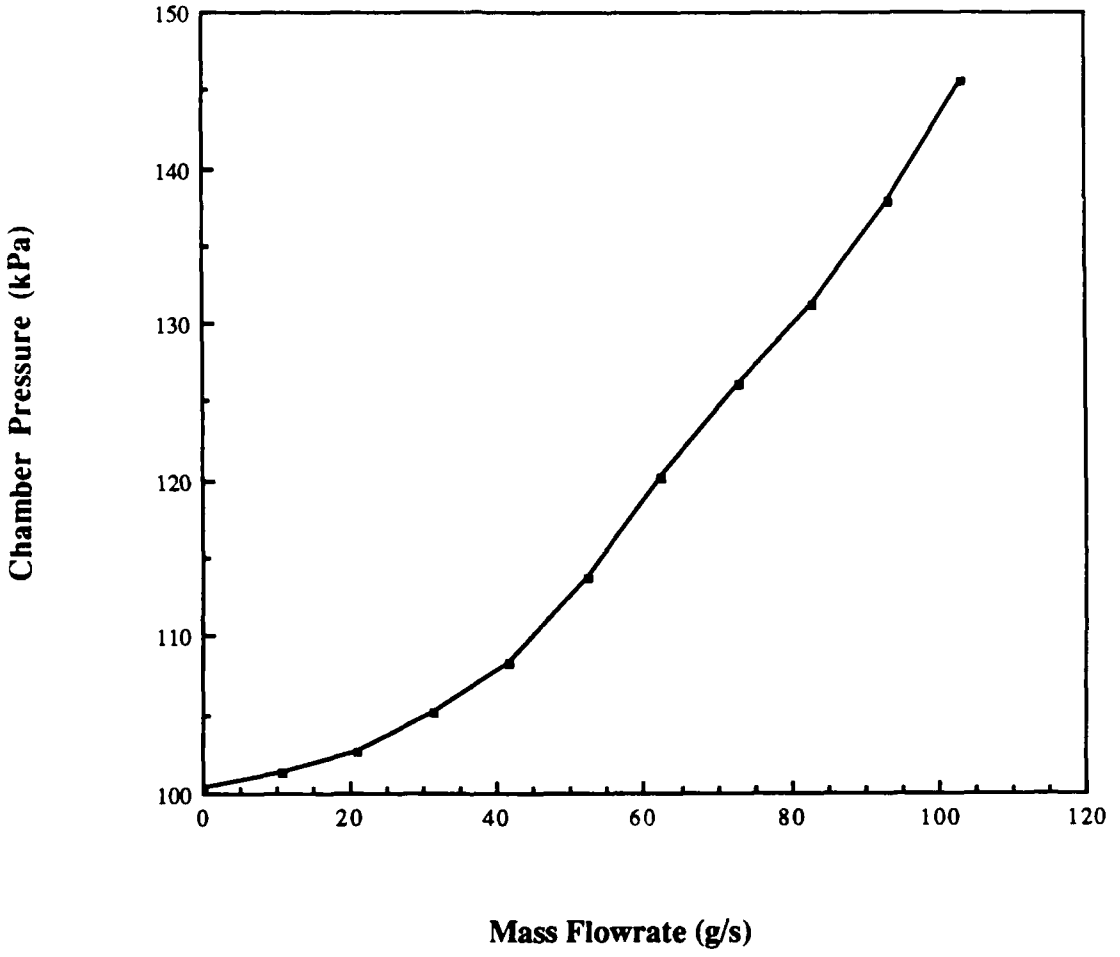

Figure 3.2 Chamber gas pressure dependence on mass flowrate. Due to restrictions in the chamber exit ports, pressure is an increasing function of mass flowrate.

3.4 Gas Temperature Measurement

The measurement of gas temperature for the purpose of determining thermal energy conversion efficiency is the focus of this investigation. Laser power absorption measurements are also made, and will be discussed in the next section.

In this study all temperature measurements made for the purpose of efficiency calculation have been made with conventional thermocouples. If the flow in the ports is kept incompressible, it is possible to make fairly accurate temperature measurements with a thermocouple. Details for making temperature measurements in the inlet and exhaust ports can be found in Reference 14.

In the chamber ports thermocouple error due to radiation and conduction heat transfer with the chamber environment is negligible if radiation shields are used. Early experiments employed thermocouples placed outside of the ports, in the interior of the chamber. Here they were exposed to high intensity plasma radiation, and direct heating from the unabsorbed laser beam. In addition the gas velocity in the chamber is substantially lower than in the exhaust ports, and therefore convective heating of the bead by the gas is not as significant. It has been shown that for most cases of interest, exhaust port thermocouples underpredict gas temperature by less than 5 K [14].

Another advantage of exhaust port temperature measurements is that the temperature can be taken as a bulk gas temperature. This assumes that the gas is well mixed after it accelerates from the chamber into the much smaller exhaust ports. This mass-averaged temperature can then be used to calculate thermal efficiency directly, avoiding the rather involved and somewhat uncertain methods required for in-chamber thermocouples.

This study has used the recommendation of McMillin and installed a shielded, fast-response type K thermocouple in each of the four exhaust ports. Each thermocouple is monitored by the Fluke system every 1.5 seconds, and the four temperatures are averaged into memory. Two of the thermocouples consistently read hotter than the other two. The

best explanation for this to date is that some flow irregularity causes the hot plume to favor one side of the chamber. Thermocouple malfunction apparently is not the cause as they have been interchanged without change in the results. Currently it is concluded that the temperature measurements are valid representations of actual gas temperature in the exhaust ports.

3.5 Absorption Measurements

One important aspect of studying LSP's is trying to determine how much of the incident laser power is absorbed by the plasma. An understanding of the variation in absorption with changing operating conditions is essential for studying and understanding thermal energy conversion processes. For example if a change in operating conditions brings about an increase in absorption, but a decrease in efficiency, most likely an increase in radiation loss has occurred.

It is generally believed that nearly complete absorption of the incident laser power is required to make laser propulsion practical. Already absorption fractions up to 85% have been reported for input powers of less than 10 kW [16]. The trends indicate increasing absorption for increasing power, and it is expected that the very high powers required for laser propulsion will facilitate nearly complete absorption.

All the absorption results presented here have been compiled using a conventional calorimetric technique. A water-cooled copper cone calorimeter is mounted to the top of the chamber and collects laser energy which is not absorbed by the plasma. It is assumed for analytic simplicity that laser energy scattered by the plasma and plasma irradiation of the calorimeter are negligible. Laser energy scattered by the plasma (not transmitted to the calorimeter or absorbed by the plasma) can be shown to be less than 2% for the electron number densities in these experiments [4]. To date no method has been devised to estimate the plasma irradiation effect on measured absorption.

Another effect which contributes to absorption measurement uncertainty is calorimeter heating by the hot exhaust gas. In the past a sodium chloride window has been used to separate the calorimeter from the gas flow, while allowing transmission of the laser beam. This method requires fairly precise knowledge of window transmission, which is difficult to acquire in this instance. Windows mounted on top of the chamber become much hotter much faster than the laser inlet window. This condition tends to crack the windows rather quickly, adding to the power transmission uncertainty. Even without cracking, power losses in salt windows are more uncertain at high temperature.

In this investigation high pressure experiments preclude the use of a window atop the chamber altogether. The pressure differential created across the sealed window would cause the window to fail immediately in all cases. Indeed, even in some cases of atmospheric chamber pressure but very high gas velocity, the window cracks badly, rendering the method useless. There are, however, a limited number of experiments that were done with a window in place at one atmosphere and intermediate flow velocities. The efficiency calculations from these cases are instructive as to the absorption behavior.

Consider a case in which placing a window atop the chamber chamber results in a 2% increase in measured thermal efficiency (e.g. 20% to 22%). This indicates that 2% of the incident laser energy was being converted to gas thermal energy, but then was lost into the calorimeter while not isolated by a window. It follows that this 2% of the incident energy was interpreted by the calorimeter as directly transmitted laser energy. So if the calorimeter measures 24% transmission without a window (76% absorption), it can be deduced that actual transmission was 22%. Again, this is ignoring the effects of scattering and plasma irradiation.

In all the cases run with a window atop the chamber, the gain in measured thermal efficiency was less than 3%. This error is approximately equal to the error scattering induces (<2%), and in the opposite sense, so tending to cancel. The generality of this

argument coupled with the lack of a good estimate for plasma irradiation of the calorimeter lead to skepticism concerning the absolute magnitudes measured for absorption percentages. However, it is believed that they are accurate enough to provide an excellent interpretative tool when comparing the overall effect of one set of operating conditions to another.

The calorimeter is equipped with two arrays of thermocouples, one each for measuring inlet and outlet water temperature. The difference in these temperatures represents the amount of energy transmitted by the plasma, and has been calibrated against known input laser powers. The Fluke system is programmed with this linear calibration, and calorimeter output voltages are stored as transmitted laser energy.

3.6 Thermal Conversion Efficiency Calculation

As stated earlier, the key issue in this study is the measurement and characterization of the thermal conversion efficiency of a laser-sustained plasma. The thermal efficiency, η_{th}, is defined as the fraction of the input laser power retained by the working gas.

In this study thermal efficiency is determined by measuring the enthalpy flux (Watts) of the inlet and exhaust gas. The difference between these two measurements is divided by the inlet laser power to give the fraction of laser energy retained by the working gas. That is,

$$\eta_{th} = (100)\dot{\Delta H}/P_L \tag{3.3}$$

where the change in enthalpy flux, $\dot{\Delta H}$, is given by,

$$\dot{\Delta H} = \dot{m} C_p (\overline{T}_{o,exit} - \overline{T}_{o,inlet}) \tag{3.4}$$

In this expression $\dot{m}$ is the mass flow rate (kg/s), C_p is the specific heat of the working gas (J/kgK), and $\overline{T}_o$ is the measured mass-averaged temperature. The greatest difficulty is accurately measuring the exit gas temperature.

As mentioned in section 3.4, there is a fast response thermocouple in each of the four exhaust ports. Assuming the gas is well mixed, the gas temperature measured in the ports is ideally the mass-averaged plasma exit temperature. However, this analysis results in an overall system thermal efficiency. The plasma exit gas experiences convective losses to the relatively cold environment before the gas temperature is measured in the exhaust ports. This is an experimental shortcoming that cannot be overcome by using in-chamber thermocouples, as discussed in section 3.4.

The effects of the gas heat losses will be discussed further in Chapter 4. Obviously, as the temperature difference between the plasma exit gas and the chamber environment becomes greater, so does the potential for heat loss. The operating conditions which effect the exit gas temperature along with wall temperature estimates must be carefully considered when interpreting the data.

Convective heat losses are difficult to quantify. This dilemma points up the need for a non-intrusive temperature measurement technique such as Laser Induced Florescence (LIF). This technique could theoretically be used to measure both temperature and velocity fields immediately downstream of the plasma and would allow a determination of plasma exit enthalpy flux before significant heat losses have occurred. This concept is currently under development for use on this project, and further details can be found in Reference 1.

4. Results and Discussion

The results to be presented and discussed here will concern the experiments with high velocities (>9m/s) and those with elevated pressure (up to 40 psia). The effects of experimenting under various operating conditions will be assessed and the progress toward the goal of determining the set of all optimal operating conditions will be discussed.

In the scope of this investigation numerous experimental parameters can be varied. Laser power, flow velocity, and chamber pressure are the parameters of current interest. Optical f-number is also known to have an effect on plasma behavior, but only f/7 (single plasma) data is to be presented in this work. The end of this chapter will contain a discussion of multiple plasma results and the implications for future work in that area.

The concept of optimal operating condition can be thought of as the mass flux (kg/sm^2) for which a given combination of laser power, chamber pressure, and f-number produces the highest thermal conversion efficiency. Mass flux is determined by the quantity, ρu, where ρ is the gas density and u is gas velocity. By the relation,

$$\dot{m}=\rho u A \tag{4.1}$$

where $\dot{m}$ is the mass flow rate (kg/s), and A is the flow area (m^2),

$$\rho u=\dot{m}/A \tag{4.2}$$

gives mass flow rate per unit area (mass flux).

4.1 High Velocity Experiments

The addition of the sintered steel flow straightener and converging quartz tube have

allowed experiments at atmospheric pressure with velocities over 9 m/s at powers to 7 kW.

Figures 4.1 and 4.2 show the variation in thermal efficiency and global absorption percentage respectively with mass flux for four different power plasmas up to 7 kW. The chamber pressure is one atmosphere. The measured efficiencies range from 11% at low mass flux and 7 kW, to 35% at high mass flux and 2.5 kW In this range of mass flux there is a clear upward trend in efficiency with increasing mass flux. It is important to realize that this data was taken with the 49 mm diameter quartz tube in place, which presents a condition susceptible to significant heat losses from the plasma exit gas. (These losses will be discussed in section 4.3). The trends described by the data in Figure 4.1 are believed to be valid, but the magnitudes should be considered in light of the information in section 4.3.

The absorption curves in Figure 4.2 for all the plasmas appear to peak between 5.97 kg/sm^2 and 8.95 kg/sm^2, and then level off somewhat. At a quartz tube throat diameter of 49 mm, this gives mean velocities of 3.7 m/s and 5.6 m/s respectively. The lower power plasmas peak at lower mass fluxes than do higher power plasmas. The maximum absorption recorded for any case is 87% at 7 kW and 8.95 kg/sm^2.

Figure 4.3 is a comparison between a 2.5 kW and a 4 kW plasma at a mass flux of 5.97 kg/sm^2. Careful inspection reveals that the 4 kW plasma front is lower (further upstream) than the 2.5 kW plasma front. In this case the higher power plasma front is over 4 mm lower than the lower power front. Since higher power plasmas appear to have an absorption peak at higher mass fluxes than lower power plasmas, Figure 4.3 would indicate that plasma front position relative to the laser focus is an important parameter for optimizing global absorption percentage. In addition Figure 4.2 shows overall higher absorption for higher power plasmas, which indicates the potential for higher thermal conversion efficiency.

One would expect that if absorption begins to decline after a certain mass flux is reached at a given power, the thermal efficiency would also begin to decline. Figure 4.1

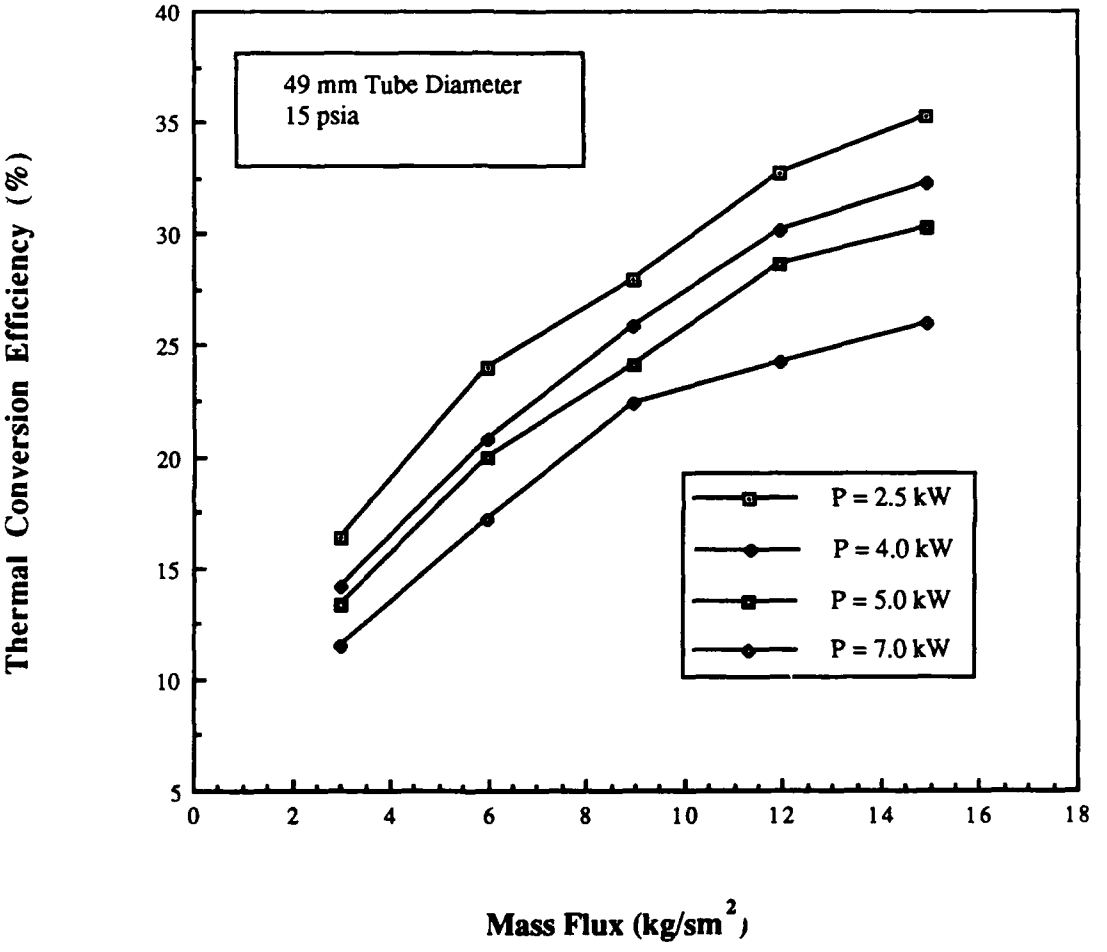

Figure 4.1 Thermal conversion efficiency as a function of mass flux for plasmas at one atmosphere gas pressure. Results are shown for four different input laser powers.

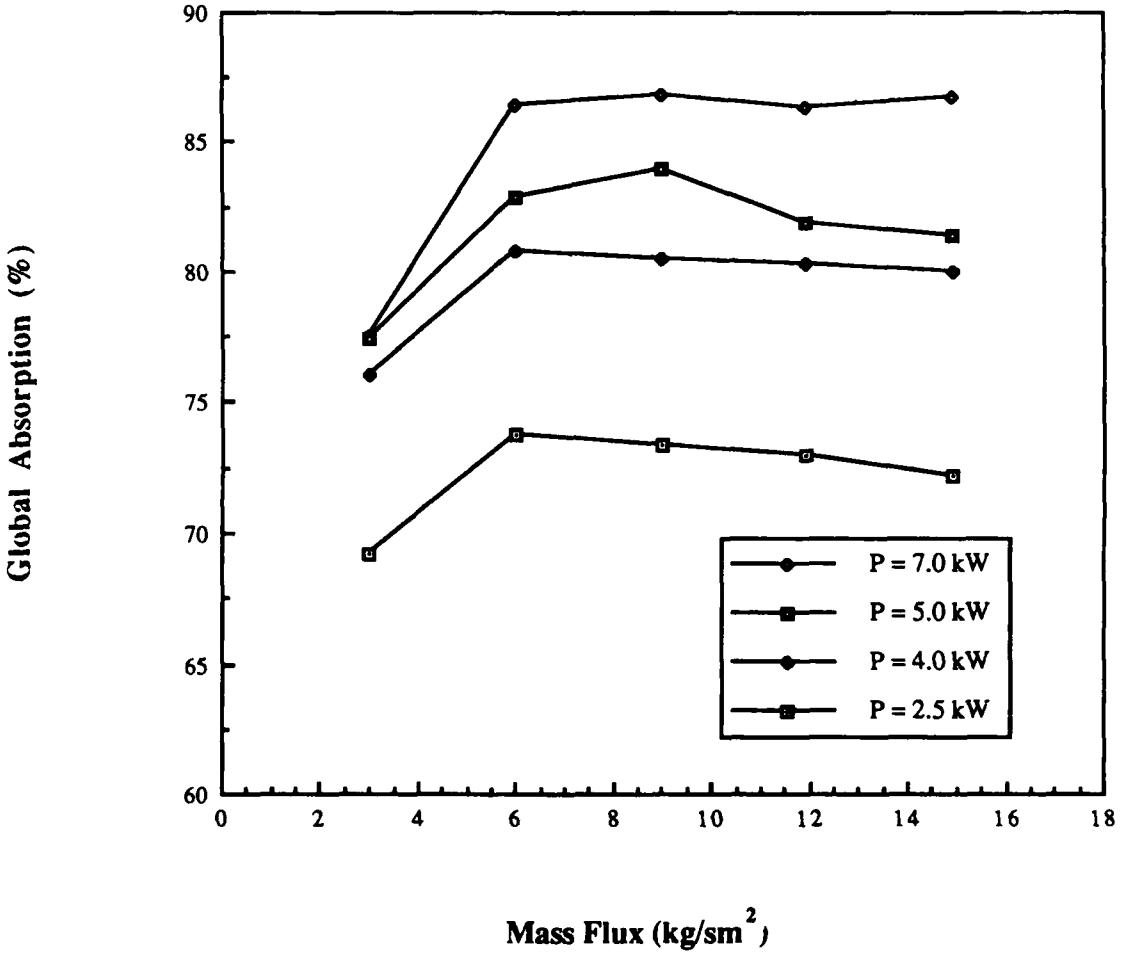

Figure 4.2 Global absorption percentage as a function of mass flux at one atmosphere gas pressure. Results are for four different input laser powers.

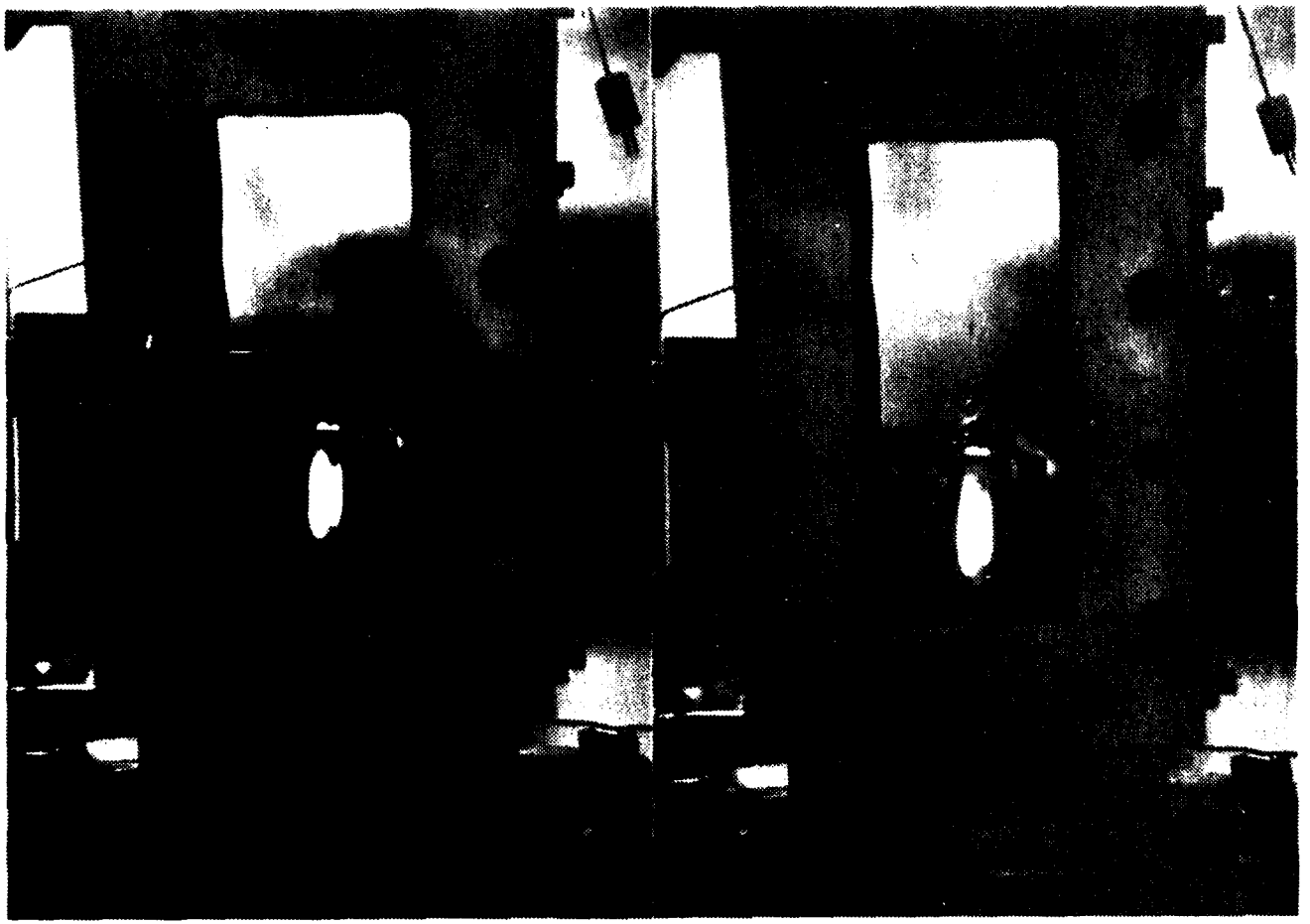

2.5 kW 4.0 kW

Figure 4.3 Comparison between the plasma position for two different laser powers at constant mass flux. The focus position was lowered 50 mm from tungsten rod (shown in left photograph). The window ledge is a convenient reference location.

shows that this is clearly not the case. For all laser powers tested, efficiency continues to increase with mass flux. It also appears to decrease with increasing laser power at a given mass flux. This behavior is due to the variation in radiated energy with mass flux and power. The increasing efficiency indicates that there is a decrease in radiation from the plasma at higher mass flux, which in this case more than offsets the decrease in global absorption. Both of these decreases are presumably due to a cooler plasma at elevated mass flux.

This series of experiments must be extended to even higher mass fluxes in order to determine where the peak in efficiency occurs for each laser power. Also, an attempt to determine at what mass flux a given input power can no longer sustain a plasma (i.e. blowout) must be undertaken.

The theoretical model of Glumb and Krier [15] indicates that the higher the input power to a plasma, the higher the mass flux required to blow it out. In addition it seems a higher power plasma can eventually result in a higher peak efficiency, presumably due to its inherently higher absorption percentage. This trend will hopefully be verified with experiments intended to optimize the mass flux for a given laser power.

It should be noted that these results are for an f/7 focusing geometry and one atmosphere. It is believed that for different geometries, the energy conversion trends are similar, but some specific behavior may vary. For instance one finds in Reference 16 the results of an f/3.5 focusing geometry, and the peak in absorption occurs at the very lowest end of the mass flow range for all available laser powers. This is in contrast to the initial rise in absorption at f/7, which is then followed by a gradual decline.

4.2 Elevated Pressure Experiments

For actual laser propulsion rocket thruster chamber pressures above several atmospheres will be required for adequate performance. It is important then to characterize

plasma behavior under various chamber pressures and try to determine ways in which to optimize thermal energy conversion.

In our experiments we have elevated the gas pressure to as high as 40 psia for powers up to 7 kW and mass flux up to 11.93 kg/sm^2. It can be seen from Figure 4.4 that the plasma displaces upstream and becomes smaller with increasing pressure. As pressure increases the plasma moves further upstream of the laser focus due to an increase in absorption coefficient. However, the shift into a region of lower beam intensity, along with a decrease in plasma size results in the decrease in overall absorption fraction shown by the data in Figure 4.5.

This result is in contrast to predictions that the increase in absorption coefficient associated with elevated gas pressure should give rise to an increase in overall absorption. It seems clear that the mass fluxes used to this point have been inadequate to produce well-matched operating conditions for elevated chamber pressures. Running experiments at elevated pressure and much higher (double or triple current maximum) mass flux should help correct for the plasma shift and size decrease seen in Figure 4.4. It is hoped that global absorption fractions as high or higher than those seen at one atmosphere can be realized.

Figure 4.6 shows the resultant decrease in thermal efficiency with increasing pressure at constant mass flux. At 4 kW efficiency drops from 26% at 15 psia down to 14% at 40 psia. The decrease in global absorption coupled with a pressure related increase in radiative emission coefficient [1] reduces the thermal conversion efficiency significantly. Experiments at elevated mass flux will be helpful in understanding the relationship between the operating conditions and the energy conversion fractions.

Figure 4.7 shows that at a given input laser power, plasma global absorption is increasing with increasing mass flux. This appears to be a result of pushing the plasma closer to the focus, representing a better matched set of operating conditions. Again,

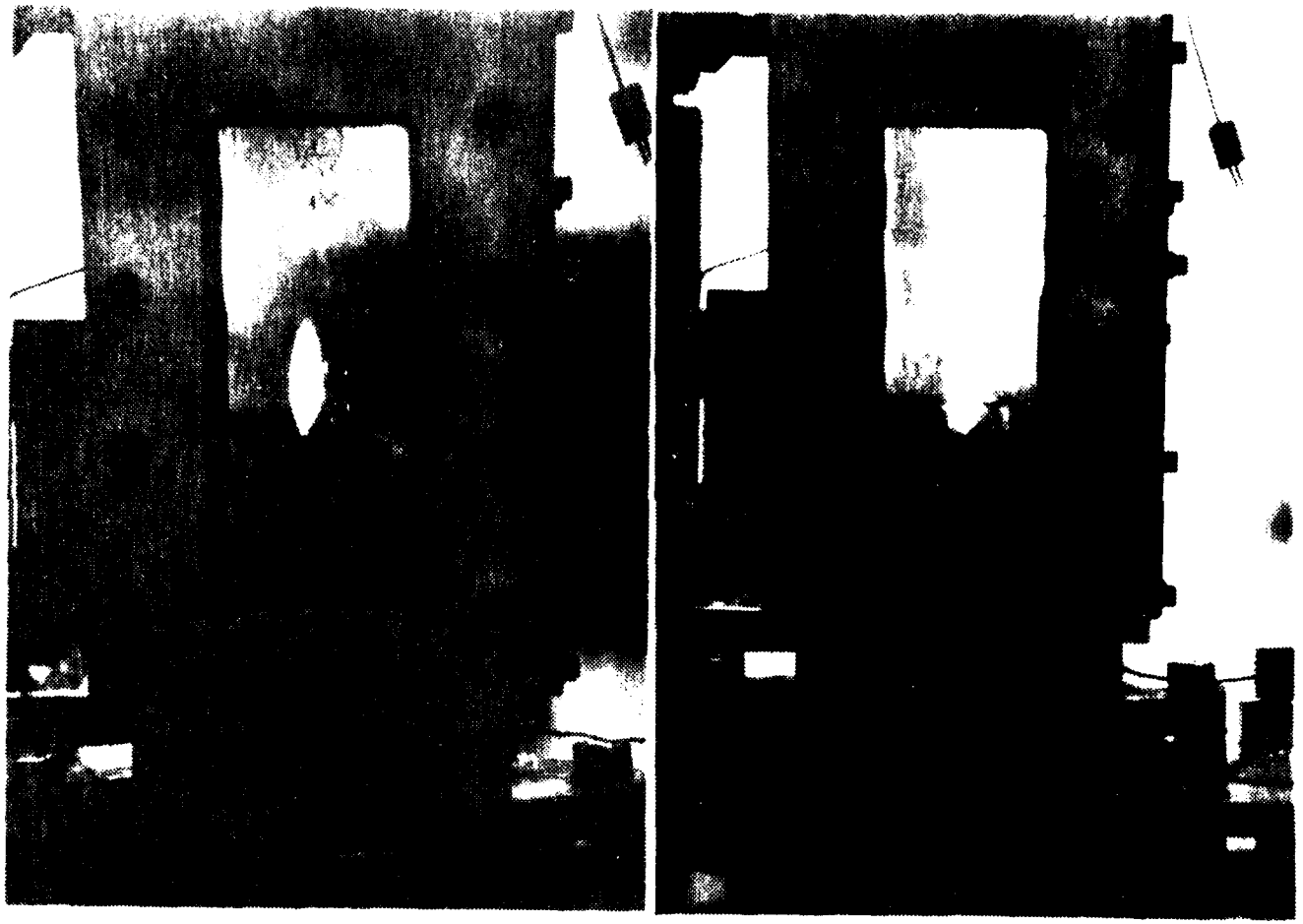

15 psia 29 psia

Figure 4.4 Comparison between the plasma position for two different gas pressures at a mass flux of 8.95 kg/sm^2. Neither plasma has been manually lowered from its initiation position. The laser power is 5 kW in both cases. The lip of the quartz tube is a convenient reference location.

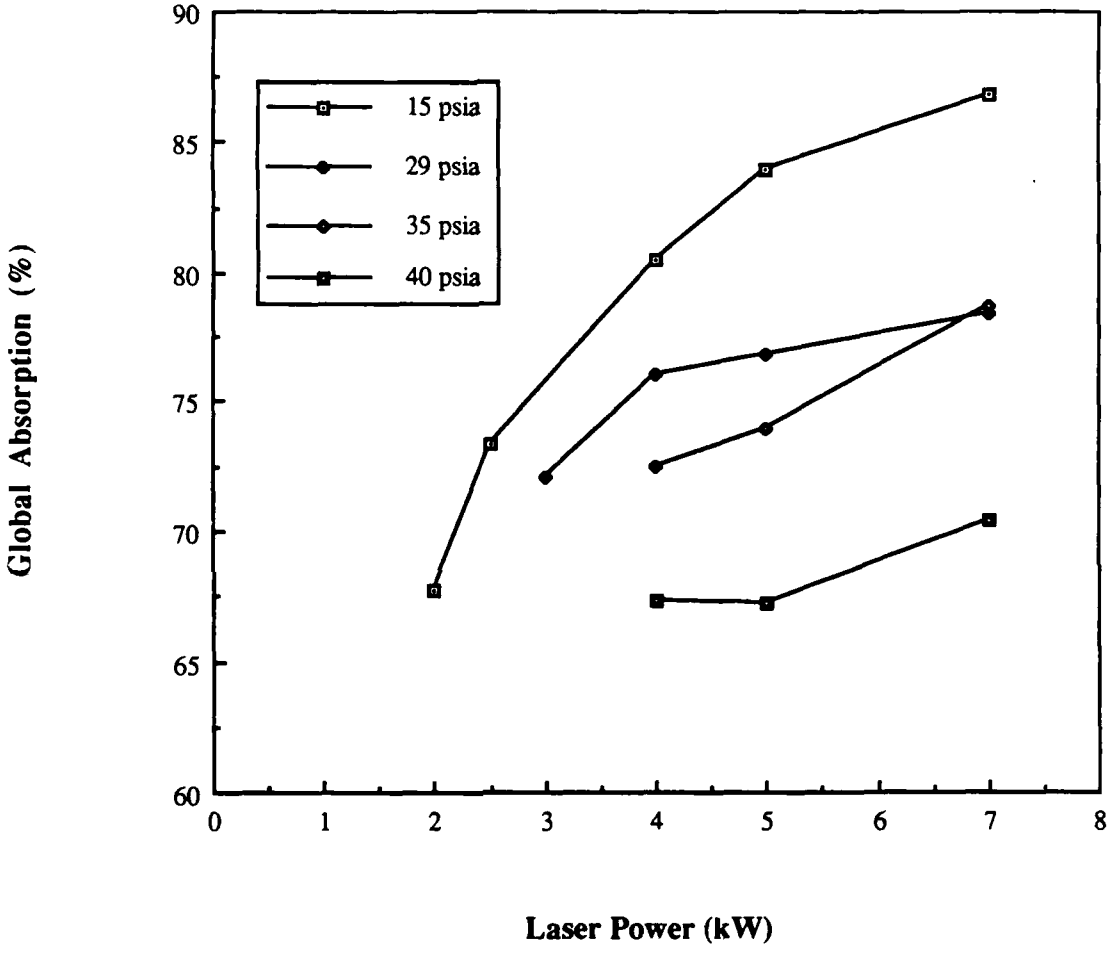

Figure 4.5 Global absorption percentage as a function of input laser power. The mass flux is 8.95 kg/sm^2 in all cases. Results are shown for four different gas pressures.

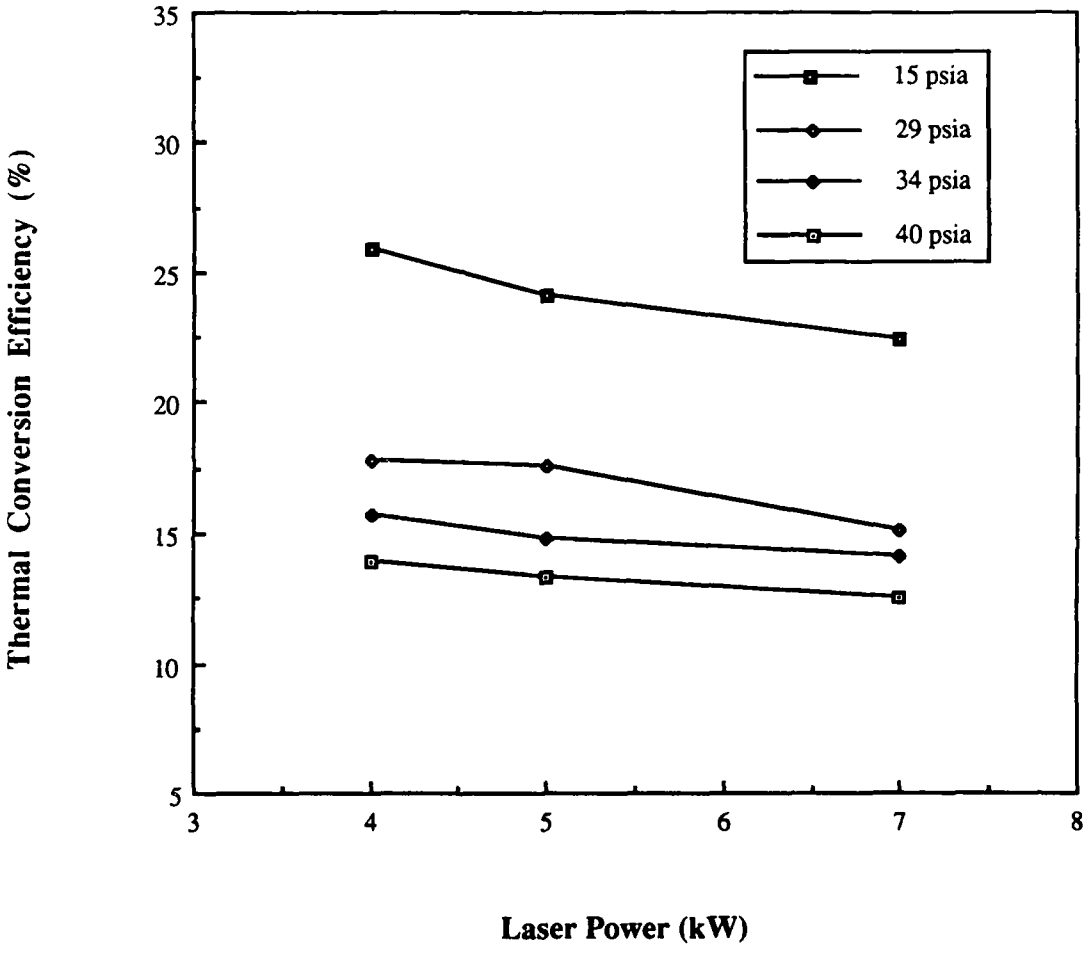

Figure 4.6 Thermal Conversion efficiency as a function of laser power. The mass flux is 8.95 kg/sm^2 in all cases. Results are shown for four different gas pressures.

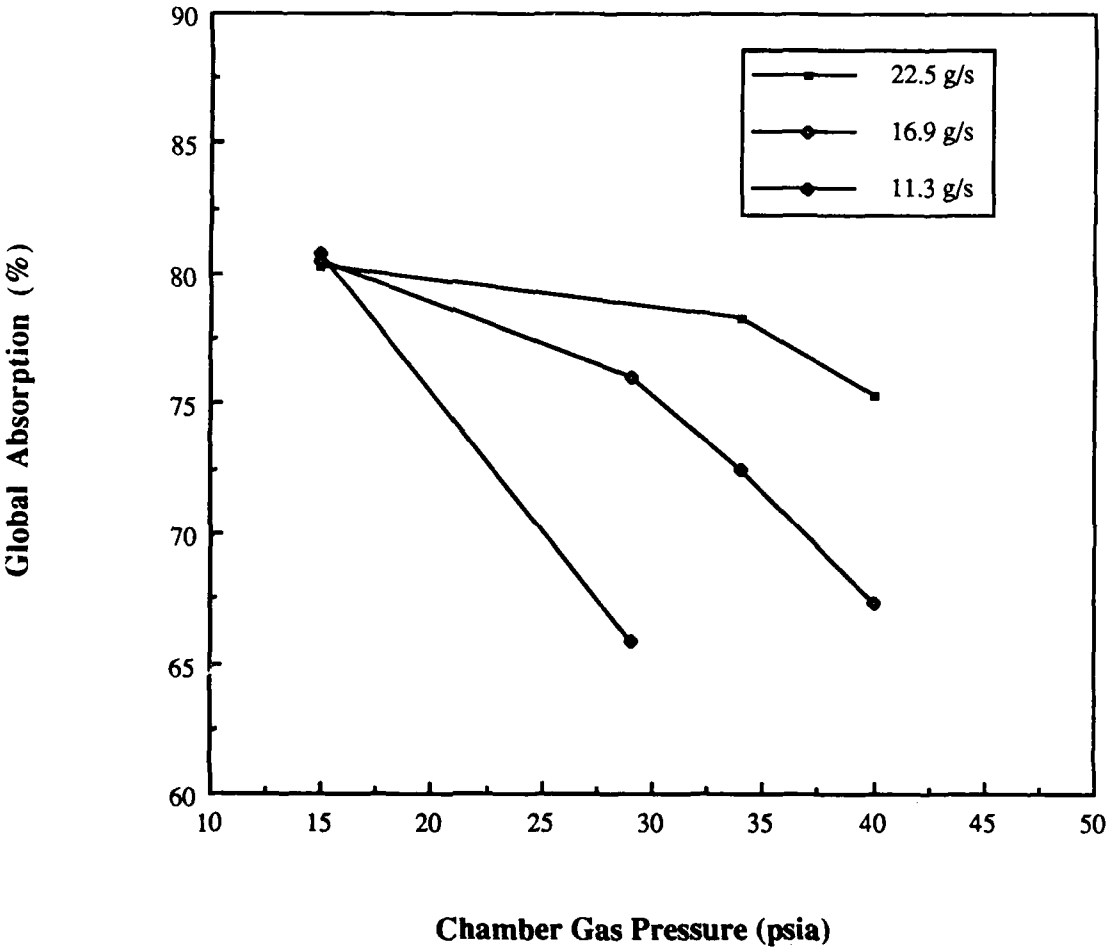

Figure 4.7 Global absorption percentage as a function of chamber gas pressure. The input laser power is 4 kW in all cases. These experiments were done with the 49 mm quartz tube in place, and results are shown for three different mass flowrates.

higher mass fluxes should be used in an attempt to optimize the operating conditions with respect to global absorption fraction, and more importantly, thermal conversion efficiency.

4.3 Heat Loss from Exit Gas

As mentioned in section 4.1, the experimental set-up involving the high velocity and elevated pressure tests is prone to substantial heat loss from the exit gas. These losses take place before the exit gas temperature is measured in the exit ports, and as a result artificially low thermal conversion efficiencies are calculated.

Figure 4.8 presents data comparing measured thermal efficiency using two different flow configurations. All the points below 2.98 kg/sm^2 are data taken without a converging quartz section in the chamber, and the points above 2.98 kg/sm^2 are with a 49 mm diameter quartz section in place. The obvious discontinuity in the data appears to be due to significantly higher heat losses from the plasma exit gas when using the converging quartz section. For instance at 5 kW there is approximately an 8% drop in efficiency when going to the quartz tube geometry, representing a loss of about 400 W. Almost seven times less mass flow (kg/s) is required to achieve a given mass flux (kg/sm^2) with the quartz section than without, due to the area decrease. Theoretically, plasmas operated at equal mass flux should exhibit the same thermal efficiency (all other things being equal). This implies that the exit gas of a plasma sustained in the quartz tube must produce a bulk temperature rise almost seven times greater than a plasma in the open chamber. This becomes clear in view of this relationship between the energy retained by the gas for each case,

$$\dot{m}_1 C_p \Delta \overline{T}_{o,1} = \dot{m}_2 C_p \Delta \overline{T}_{o,2} \qquad (4.1)$$

A (1) subscript denotes the open chamber, and a (2) subscript denotes the converging quartz tube. Since the mass flow in (1) is a constant factor times the mass flow in (2), the

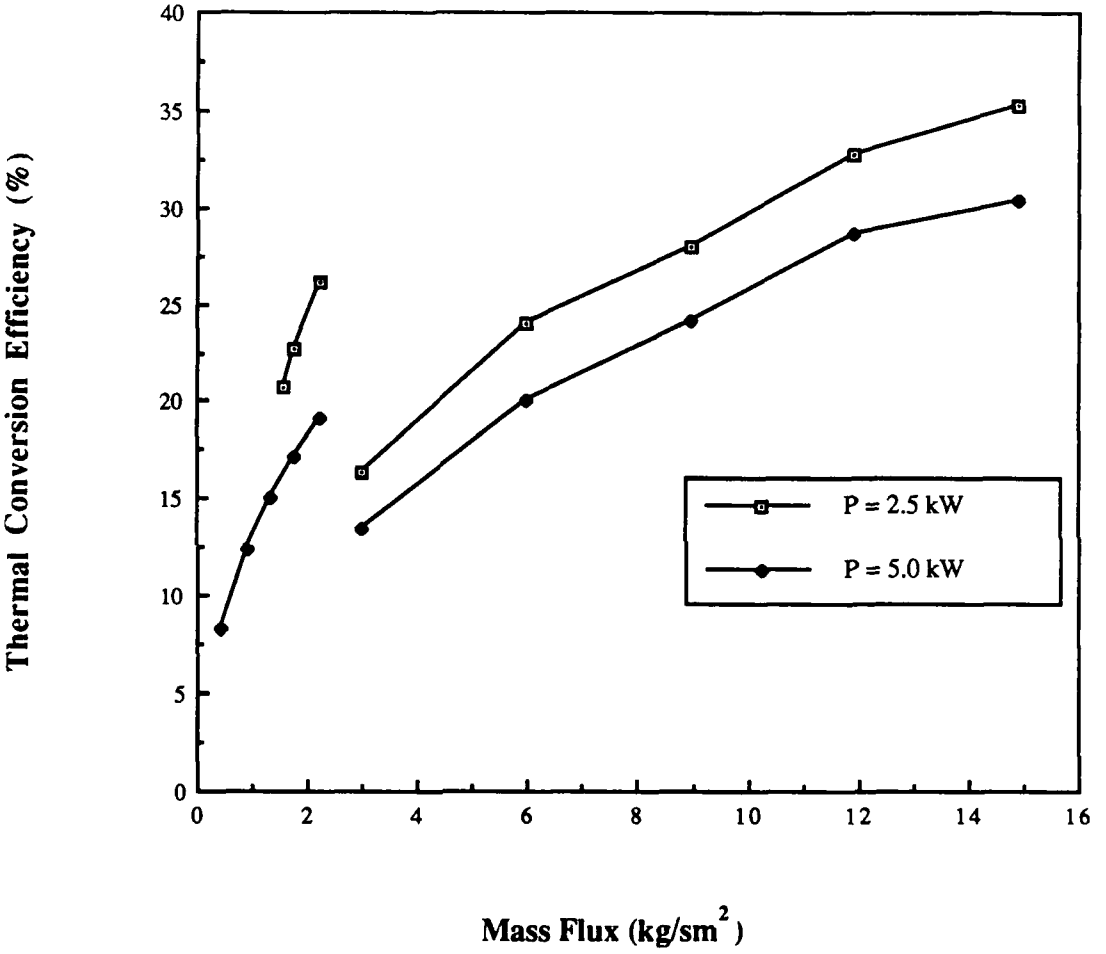

Figure 4.8 Thermal conversion efficiency as a function of mass flux at one atmosphere gas pressure. Shows the difference between measured efficiency with (curves on right side) and without the 49 mm quartz tube in place. Results are shown for two input laser powers.

temperature rise in (2) must be the same constant factor times the temperature rise in (1). In this case the constant factor is slightly less than seven.

We believe that the dominant heat loss mechanism from the gas is convection to the exit port and chamber walls. Radiation is thought to be insignificant at the gas temperatures existing here.

Convection loss is difficult to quantify in this experimental set-up for various reasons. In order to make an accurate estimate of the convection coefficient, fairly precise knowledge of the flowfield and the boundary conditions is required. In our system the flowfield is not well characterized with respect to its velocity and temperature fields. Also, the boundary condition can neither be considered constant heat flux nor constant temperature as would be necessary for most convection analyses.

Several experiments have been undertaken in an attempt to understand the general nature of the convection losses observed. It was first thought that large recirculation zones in the main chamber brought about by the jet nature of the quartz tube geometry were enhancing losses to the main chamber walls. In contrast in the open chamber smooth cool flow goes over the walls with very little convection loss.

To check this theory, a horizontal plate was inserted into the chamber near the lip of the quartz tube. The idea behind this was to reduce the size of the recirculation zones and hence, the convection losses. The resultant change in measured efficiency was negligible, leading to the conclusion that convection from recirculation zones is not the source of the discontinuity seen in Figure 4.8.

Closer inspection of experimental data revealed that experiments done with the plasma lowered into the quartz tube resulted in much lower main chamber wall temperatures. This was thought to be a possible cause of enhanced losses due to a greater gas-wall temperature differential. Subsequently, several tests were made with the plasma just at the lip of the quartz to test this theory. At this location in the chamber the plasma is still subjected to the

same mass flux as in the tube, but radiates directly to the chamber wall rather than to the quartz. These tests resulted in a much hotter chamber wall, but the efficiency remained unchanged. This result, in conjunction with the recirculation zone results, gives evidence that the bulk of the convection losses occur in the exit ports rather than the main chamber.

The exit ports present a geometry that can be looked at qualitatively from an analytical point of view. The irregular main chamber flow is being accelerated into the ports, creating a much more uniform, tractable situation.

Even though the Reynolds number for all of the mass flows encountered here exceed the critical value of 2300, the flow cannot be considered turbulent. Twenty-five to forty pipe diameters are typically required to fully develop even turbulent flow, and many more for laminar flow [21]. The exit thermocouple in our facility is only eight pipe diameters from the exit port entrance, meaning that all of the flow of interest is in the entrance region of the pipe.

Entrance region flow can be considered laminar in this situation. The transition to turbulence based on a local length Reynolds number,

$$Re_x = Ux/\nu \tag{4.2}$$

will not occur for a value of x less than 22 cm, for any case considered here. U is the freestream velocity, ν is the kinematic viscosity, and x is the distance from the entrance of the pipe. This result is for a conservative estimate of 80,000 for the value of critical length Reynolds number. In the exit port the thermocouple is only 10 cm from the exit port entrance, hence the flow is laminar for the entire length of interest.

The Nusselt number, Nu, is a dimensionless quantity representing convective heat transfer. For pipe flow it is defined as,

$$Nu_D = hD/k \qquad (4.3)$$

where h is the convection heat transfer coefficient, D is the diameter of the pipe, and k is the thermal conductivity of the fluid. Solutions have been obtained for Nusselt number in the entrance region of a pipe as a function of Reynolds number [22].

The results found in Reference 22 indicate that Nusselt number, and therefore convection heat transfer coefficient, is a weak increasing function of Reynolds number in laminar entrance region flow. Thus it is reasonable that convection losses will be a weak function of mass flow rate, while still remaining a strong function of gas-wall temperature differential. It is then clear why a discontinuity exists in the efficiency plot in Figure 4.8. Consider the two points on either side of 2.98 kg/sm^2. The point on the left is from a test in the open chamber, with a high mass flow rate and a relatively small rise in bulk gas temperature. The point on the right, with the lower efficiency, is from a test in the quartz tube. This latter test had a smaller mass flow rate, and therefore a higher rise in bulk temperature. As just discussed the mass flow rate difference between the two tests should have little effect on the relative convection loss, whereas the large difference in gas temperature should have a strong effect. The gas in the quartz tube test has most likely lost much more energy to the port wall, thereby giving the appearance of a much lower efficiency.

Even though the exit ports present a fairly small combined surface area for convective heat transfer, the entrance to the pipe has a very thin boundary layer, which remains fairly thin throughout the length of interest. In general, thin boundary layers give rise to large values of convection coefficient. It is therefore conceivable that adequate convective cooling of the plasma exit gases has taken place to produce the discontinuity in Figure 4.8.

It is difficult to check quantitatively the effect of exit port convection heat loss. The best attempt to date has been to place an unshielded thermocouple into the exit port radially

and measure gas temperature about 1/2 inch from the port entrance. Currently a radiation shield for this type of application is not available, but should be in the near future. The results of the preliminary test indicate that as much as 5% of overall efficiency may be recovered with the unshielded thermocouple, depending on the operating conditions. Further testing with shielded thermocouples will hopefully verify that the discontinuity in efficiency is caused by convection loss to the exit port walls.

It should be noted that as a test progresses the measured thermal efficiency tends to increase. In earlier work by McMillin et al., [16] a normalization procedure was utilized based on a standard main chamber wall temperature at which to record gas temperatures, and hence thermal efficiency. It appears now that exit port wall temperature is the important parameter, although one which is presently unrecorded. This leaves an additional uncertainty as to what point in a test to take an efficiency measurement. Currently the efficiency is taken when it appears that the transient rise has begun to level off, or about 90 seconds into any given test. Although this does not guarantee that an equivalent relative energy percentage has been lost, we believe this to be an adequate interpretive tool for evaluating efficiency data.

4.4 Summary of Multiple Plasma Results

In a realistic laser propulsion application laser power on the order of 10^6 to 10^9 Watts will be required. To facilitate this high power in a rocket thruster the laser beam will almost certainly have to be split for transmission through windows, since fluxes less than 10^4 W/cm^2 are current material limits. In addition to this practical rationale for beam splitting we believe that multiple plasmas can be made to operate more efficiently than a single high power plasma. It is this aspect of multiple plasmas which motivated this part of our investigation.

Figure 4.9 is a double exposed photograph of twin plasmas sustained simultaneously

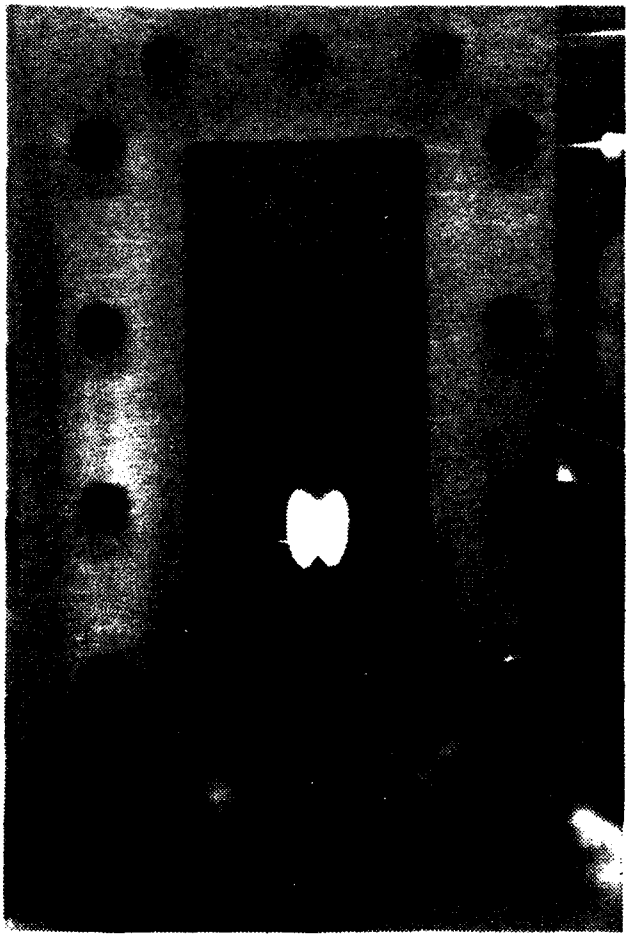

Figure 4.9 Photograph of two plasmas simultaneously sustained at 6 kW total input power.

at 6 kW total power and a mass flux of 0.45 kg/sm^2. (The chamber photograph was taken first and then the plasmas were photographed through a neutral density filter thereby exposing the film a second time.) The beam foci were separated by 12 mm, and the individual plasmas are easily distinguished. The f/2.5 off-axis optical configuration was used in these twin plasma experiments.

In preliminary experiments comparisons were made between the measured thermal efficiency of a single plasma, and the efficiency of two plasmas sustained 12 mm apart, each of 1/2 the power of the single plasma. Figure 4.10 presents the results of these comparisons as a function of total input laser power. For the lower mass flux (velocity) the single and twin plasmas display virtually the same efficiency characteristics. At the higher mass flux, however, the twin plasmas are significantly more efficient for all powers.

Experiments must be undertaken which could be used to compare the thermal efficiency of single and twin plasmas, each operated at their optimal conditions. This would give a better indication of the possible thermal advantages of multiple plasma operation. Also, comparing a given power plasma to two plasmas each of the same power as the single plasma would be of interest. It is conceivable that there are interactions between plasmas located near each other that could result in higher thermal efficiency. These interactions might include radiative transport between the plasmas, which could decrease the overall radiative loss to the chamber walls, or improved downstream thermal mixing, which has a positive impact on efficiency. A study designed to compare the variation in twin plasma separation distance could help to verify the influence of these interactions.

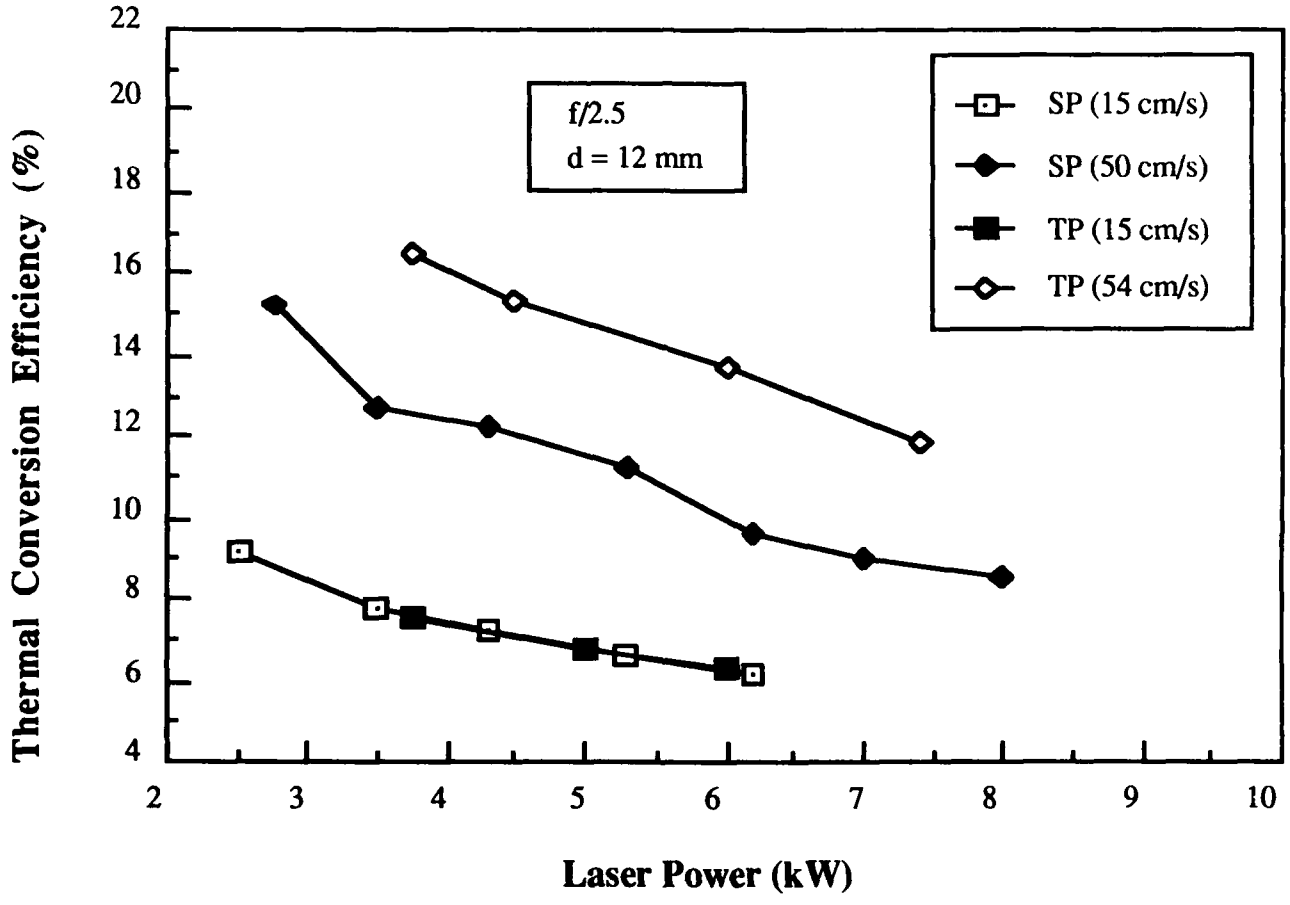

Figure 4.10 Comparison of single (SP) and twin plasma (TP) thermal efficiency as a function of total input power. The separation is distance is d; Taken from Reference 14.

5. Conclusions and Recommendations

5.1 Summary of Results

Results of experiments were presented which were not possible in earlier phases of this investigation (1984-86). Because of improvements to the gas flow system and the laser beam quality, plasmas have been tested at over 9 m/s and up to 40 psia chamber pressure. Laser input powers between 2.5 kW and 7 kW have been used with an on-axis beam focusing geometry of f/7 to initiate and sustain single plasmas. Twin and single plasmas have been sustained with an off-axis f/2.5 focusing geometry at up to 8 kW total power. Thermal energy conversion and global absorption measurements are the key quantitative results. A qualitative analysis of convection losses was performed in an effort to explain certain efficiency measurement phenomenon.

Thermal efficiency as high as 35% has been recorded for a 2.5 kW plasma at one atmosphere. This is the actual measured value and does not take into account the convection loss from the exit gas. We believe that an actual efficiency approaching 50% could be expected at these conditions if losses could be accurately accounted for. In general, efficiency tends to increase with mass flux and decrease with laser power and gas pressure at the mass fluxes currently available. The greatest thermal efficiency for a 7 kW plasma at the highest mass flux available is only 26% at one atmosphere. At 40 psia a 7 kW plasma is only 12.5% efficient (at 8.95 kg/sm^2), while at one atmosphere (15 psia) the efficiency is 22.4%. These lower values of efficiency imply that the gas mass flux supporting the plasma was more poorly matched for the higher power and the higher electron number density (proportional to pressure) experiments. The optimal thermal efficiency for a plasma at higher gas pressure will be determined in future tests.

Global plasma absorption percentage as high as 87% has been recorded by calorimetric means at a laser power of 7 kW. Plasma absorption was found to increase with laser

power and decrease with gas pressure at all available mass fluxes. The highest recorded absorption fraction for a 2.5 kW plasma at one atmosphere was only 74%. At 40 psia the peak absorption fraction for a 7 kW plasma was only 78%. There appears to be a peak in absorption percentage at one atmosphere for all laser powers used in this investigation. A mass flux ranging from 5.97 kg/sm^2 to 8.95 kg/sm^2 was found to produce this peak, depending on the laser power. A higher laser power plasma requires more mass flux to optimize global absorption.

5.2 Recommendations for Future Work

5.2.1 Experimental Apparatus

Improvements to the experimental apparatus have been mentioned in previous chapters of this work. These improvements will be summarized in this section.

Modifications to the optics system should include zinc selenide windows and lenses in place of sodium chloride for their durability and ease of maintenance. Even though zinc selenide optics are considerably more expensive as an initial investment than sodium chloride, the cost of replacing the frequently damaged sodium chloride windows is considered far greater. Another addition to the optics system should be an on-axis focusing geometry capable of splitting the laser beam for multiple plasma experiments. Remote control of the beam splitting optics should be a feature of this system so plasma separation can be controlled during an experiment.

With respect to the chamber assembly, the following improvements should be made. First a chamber pressure regulation system which provides better resolution and repeatability is needed to provide reliable gas pressure control. Also we will need to mount thermocouples to the walls of the exit ports to allow for the normalization of convection losses similar to those reported in Reference 16. Lastly, shielded, fast response thermocouples should be installed radially into the exit ports closer to the main chamber. It

is expected that the gas temperature can then be more accurately measured before significant convection heat loss has taken place.

5.2.2 Future Experiments

5.2.2.1 Mapping Optimum Energy Conversion Conditions

Experiments involving very high mass flux must be performed. First, the mass flow at which the plasma thermal conversion efficiency is optimized must be determined. This characteristic should be mapped at all available laser powers and gas pressures. The effect of varying laser beam focusing geometry on plasma behavior is also of interest. In addition the mass flux at which a plasma of a given laser power and gas pressure will extinguish, in the sense of blowout, should be found with high mass flux experiments. Also experiments designed to determine absorption tendencies at elevated pressures and much higher mass flux are necessary.

5.2.2.2 Multiple Plasmas

Preliminary experiments have indicated that using multiple plasmas may be one way of operating at high specific impulse without sacrificing thermal efficiency. Multiple plasmas should be investigated further with the goal of comparing all single/multiple plasmas at their optimal efficiencies. In addition the radiative and convective interactions of plasmas in close proximity should be investigated. We believe that energy radiated from one plasma may be absorbed by another nearby plasma, thus reducing the overall energy loss to the chamber walls.

5.2.2.3 Cold Gas Injection

Another experimental technique which may lead to increased thermal efficiency is the injection of cold gas into the downstream portion of the plasma. The cold

flow may decrease the gas temperature in the region of the plasma where only a small portion of laser energy is being absorbed. The lower plasma temperature may then result in a decrease in radiation losses, and an overall increase in thermal efficiency. This technique will require significant modification to the chamber design to allow for the cold secondary flow.

5.2.2.4 Low Molecular Weight Gases

The future of laser propulsion lies in the use of a low molecular weight gas such as hydrogen as the propellant. In this investigation we intend to initiate experiments using helium or a helium-argon mixture as the working gas. Helium typically exhibits a lower absorption coefficient than argon, and it may prove difficult to initiate and sustain a helium plasma. Based on the success of the He/Ar experiments, future work might also include experimentation with hydrogen plasmas.

5.2.2.5 Non-Intrusive Diagnostics (LIF)

As part of the ongoing laser propulsion research planar laser-induced florescence (LIF) techniques to be used for concentration and temperature mapping should be vigorously pursued. LIF is a non-intrusive diagnostic technique in which a low power laser is tuned to excite electronic transitions within an atom (usually a seed) in the flow of interest. As this atom decays to lower energy levels, the intensity of the florescent emissions can be used to determine either the concentration (giving velocity) or the temperature of the atom. By using a planar sheet of laser light to excite the seed, a two-dimensional mapping of either quantity can be obtained instantaneously.

Development of an LIF system has been underway for some time and is currently being prepared for implementation in our laboratory. This technique has the potential to provide accurate gas temperature and velocity data from directly downstream of the plasma.

With this data, measured thermal efficiency can be independently determined at various downstream locations. The effects of convection to the surroundings should be greatly reduced, and the (seemingly) minimal effect of radiative loss can be verified. LIF temperature measurements have never before been attempted in laser-sustained plasmas.

As just mentioned the calculation of thermal efficiency above the plasma requires both gas temperature and velocity information. Two different LIF techniques can be used, both of which make use of seed particles injected into the flow. Concentration of the seed atoms can be determined using a single-line LIF technique. The single-line technique makes use of a pumping laser tuned to a specific electronic transition in the seed atom. The atom's excited state then becomes well populated if the laser pumping rate is high enough. This excited state decays quite rapidly, and it is the single florescent emission from this decaying process which is detected and used to determine seed atom concentration.

The seed concentrations must be mapped over time (fairly high frame rates are required) and from these mappings seed velocity can be estimated. It is not necessary to determine the seed concentration in absolute terms in order to estimate seed velocity. All that is needed is to detect relative concentration of seed particles embedded in the gas flow.

Gas temperature can be determined using a two-line LIF technique [1]. In this technique the ratio of two distinct florescent emissions in the seed atom is determined. Temperature of the seed particles can generally be written explicitly as a function of this ratio. For this two-line technique two distinct pumping laser wavelengths are needed to excite two separate transitions of a three-level atomic system. The transitions typically share a common excited energy level, but will have different ground states. To avoid problems with laser scattering, the detection system is usually tuned to record florescence from the emission line not being excited by the laser. The two-line technique is more accurate than the single-line technique for measuring temperature.

Another possibility is to use a thermally assisted LIF technique. This technique

utilizes a single pumping wavelength and relies on a collisional process to further excite a second upper energy level. The florescence from these two emission lines can then be used in a manner similar to the two-line technique described above.

We intend to apply LIF techniques to make measurements throughout the downstream flowfield, where temperatures are expected to exceed 4000 K. At these temperatures almost all molecular seedants normally used for LIF will be dissociated, and are therefore useless. Even in regions of sufficiently low temperature, there is no guarantee that the molecules having passed through the plasma will recombine correctly downstream.

For these reasons an atomic seedant such as indium or gallium should be used in our system. These elements are monatomic and will not dissociate at high temperatures, and thus should be useful at temperatures up to their ionization temperature (about 7000 K). A further restriction on seed selection is that the seed not interfere with normal plasma behavior. If a significant number of free electrons are introduced by the seedant, absorption and emission coefficients may be artificially boosted. This is one reason sodium was never seriously considered as a seedant possibility. Indium and gallium are better choices, as they have somewhat higher ionization potentials.

6. References

1. Glumb, R.J., Ph.D. Thesis, University of Illinois at Urbana-Champaign, June 1986.

2. Glumb, R.J., and Krier, H., "Concepts and Status of Laser-Supported Rocket Propulsion," Journal of Spacecraft and Rockets, Vol. 21, No. 1, pp. 70-79, January-February 1984.

3. Caveny, L.H., Ed., Orbit-Raising and Maneuvering Propulsion: Research Status and Needs, AIAA Progress in Astronautics and Aeronautics, Vol. 89, 1984.

4. Rockstroh, T.J., Ph.D. Thesis, University of Illinois at Urbana-Champaign, October 1986.

5. Wheeler, C.B., and Fielding, S.J., "Absorption of Infrared Radiation as a General Technique for Determination of Plasma Temperature," Plasma Physics, Vol. 12, pp. 551-564, 1970.

6. Stallcop, J.R., "Absorption Coefficients of a Hydrogen Plasma for Laser Radiation," Journal of Plasma Physics, Vol. 11, pp. 111-129, 1974.

7. Oettinger, P.E., and Bershader, D., "A Unified Treatment of the Relaxation Phenomenon in Radiating Argon Plasma Flows," AIAA Journal, Vol. 5, pp. 1625-1632, September 1967.

8. Kozlov, G.I., Kuznetsov, V.A., and Masyukov, V.A., "Radiative Losses by Argon Plasma and the Emissive Model of a Continuous Optical Discharge," Soviet Physics JETP, Vol. 39, pp. 463-468, September 1974.

9. Jeng, S.M., and Keefer, D., "Influence of Laser Beam Geometry and Wavelength on Laser-Sustained Plasmas," AIAA Paper No. 87-1409, June 1987.

10. Fowler, M.C., and Smith, D.C., "Ignition and Maintenance of Subsonic Plasma Waves in Air by CW CO_2 Laser Radiation," Journal of Applied Physics, Vol. 46, pp. 138-150, January 1975.

11. Keefer, D., Crowder, H., and Peters, C., "Laser Sustained Argon Plasmas in a Forced Convection Flow," AIAA Paper No. 85-0388, January 1985.

12. Van Zandt, D.M., McCay, T.D., and Eskridge, R.H., "An Experimental Study of Laser Supported Hydrogen Plasmas," AIAA Paper No. 84-1572, June 1984.

13. Krier, H., Mazumder, J., Rockstroh, T.J., Bender, T.D., and Glumb, R.J., "Continuous Wave Laser Gas Heating by Sustained Plasmas in Flowing Argon," AIAA Journal, Vol. 24, No. 10, pp. 1656-1662, October 1986.

14. McMillin, B.K., M.S. Thesis, University of Illinois at Urbana-Champaign, August 1987.

15. Glumb, R.J., and Krier, H., "Two-Dimensional Model of Laser-Sustained Plasmas in Axisymmetric Flowfields," AIAA Journal, Vol. 24, No. 8, pp. 1331-1336, August 1986.

16. McMillin, B.K., Zerkle, D.K., Glumb, R.J., Krier, H., and Mazumder, J., "Energy Conversion in Laser Sustained Argon Plasmas for Application to Rocket Propulsion," AIAA Paper No. 87-1459, June 1987.

17. Mazumder, J., Krier, H., Rockstroh, T.J., Glumb, R.J., McMillin, B.K., Zerkle, D.K., Chen, X., "Laser Sustained Plasmas for Application to Rocket Propulsion," Technical Report, Department of Mechanical and Industrial Engineering, University of Illinois at Urbana-Champaign, UILU-ENG-87-4002, March 1987.

18. Bender, T.D., M.S. Thesis, University of Illinois at Urbana-Champaign, August 1985.

19. Schwartz, S., "Energy Conversion Experiments with Laser-Sustained Argon Plasmas: Results and Operating System Update," ME 393 Final Report, Department of Mechanical and Industrial Engineering, University of Illinois at Urbana-Champaign, December 1987.

20. Liepmann, H.W., and Roshko, A., Elements of Gasdynamics, John Wiley & Sons, Inc., 1957.

21. Chapman, A.J., Heat Transfer, Fourth Edition, Macmillan Publishing Company, 1984.

22. Kays, W.M., Convective Heat and Mass Transfer, McGraw-Hill, 1966.

23. Melles Griot, Optics Guide 3, pp. 36-37, Melles Griot, 1985.

7. Appendix A: Spot Radius Equations

Assuming that spherical abberation and diffraction angular radii are simply additive, then

$$\theta = \theta_a + \theta_d \tag{7.1}$$

where θ is the on-axis spot angular radius, θ_a is the abberation contribution and, θ_d is the diffraction contribution. Linear spot radius is then also additive for small angles. The on-axis spot angluar radius can be written as

$$\theta = (1/2)K_N(D/f)^3 + 1.22\lambda/nD \tag{7.2}$$

using a third order approximation for abberation and the standard circular aperture diffraction term [23]. In this equation n is the index of refraction of the surrounding medium (n=1 for air), D is the aperture diameter, f is the lens focal length, λ is the wavelength of the laser light, and K_N is defined as

$$K_N = (N^2\text{-}2N+2/N)/32(N\text{-}1)^2 \tag{7.3}$$

where N is the ratio of the lens index of refraction the the medium index of refraction [23].

In the small angle limit we can get linear spot radius by the relation

$$r = f \tan\theta \approx f\theta \tag{7.4}$$

where r is linear spot radius. Using equations 7.2 and 7.4 and rearranging to put r in terms of optical f-number (equation 1.2),

$$r = K_N D/2(f/D)^2 + 1.22\lambda(f/D)/n. \qquad (7.5)$$

In this work, D is 76.2 mm, λ is 10.6 μm (0.0106 mm), the index of refraction of the sodium chloride lens is 1.491, and air is the surrounding medium. To produce Figure 1.6 equation 7.5 was evaluated for a large number of f-numbers giving linear spot radius (mm) as a function of f-number.

8. Appendix B: Lens and Window Holder Drawings

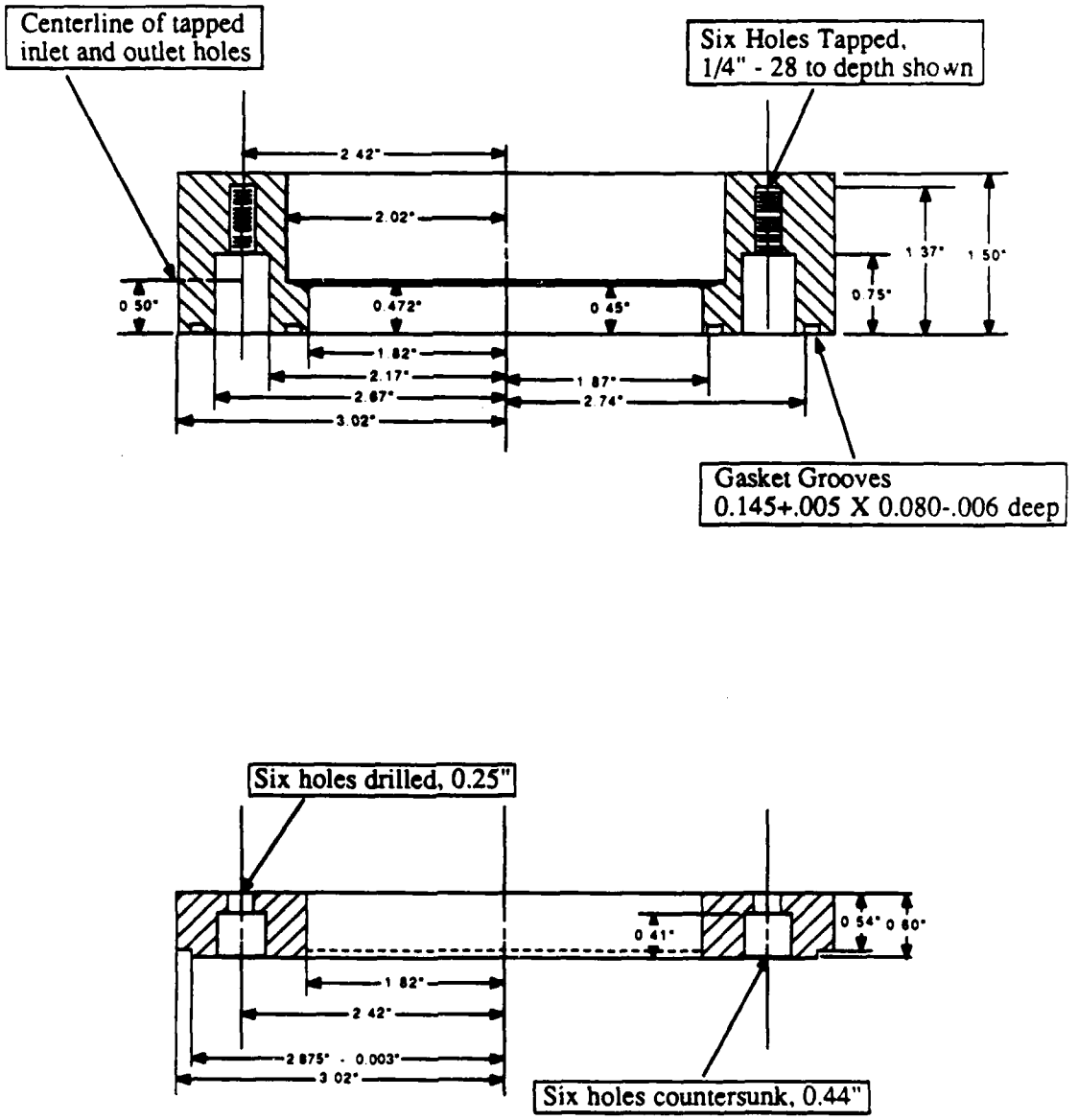

Figure 8.1 Cross sectional view of a water-cooled aluminum lens holder for zinc selenide or sodium chloride lenses.

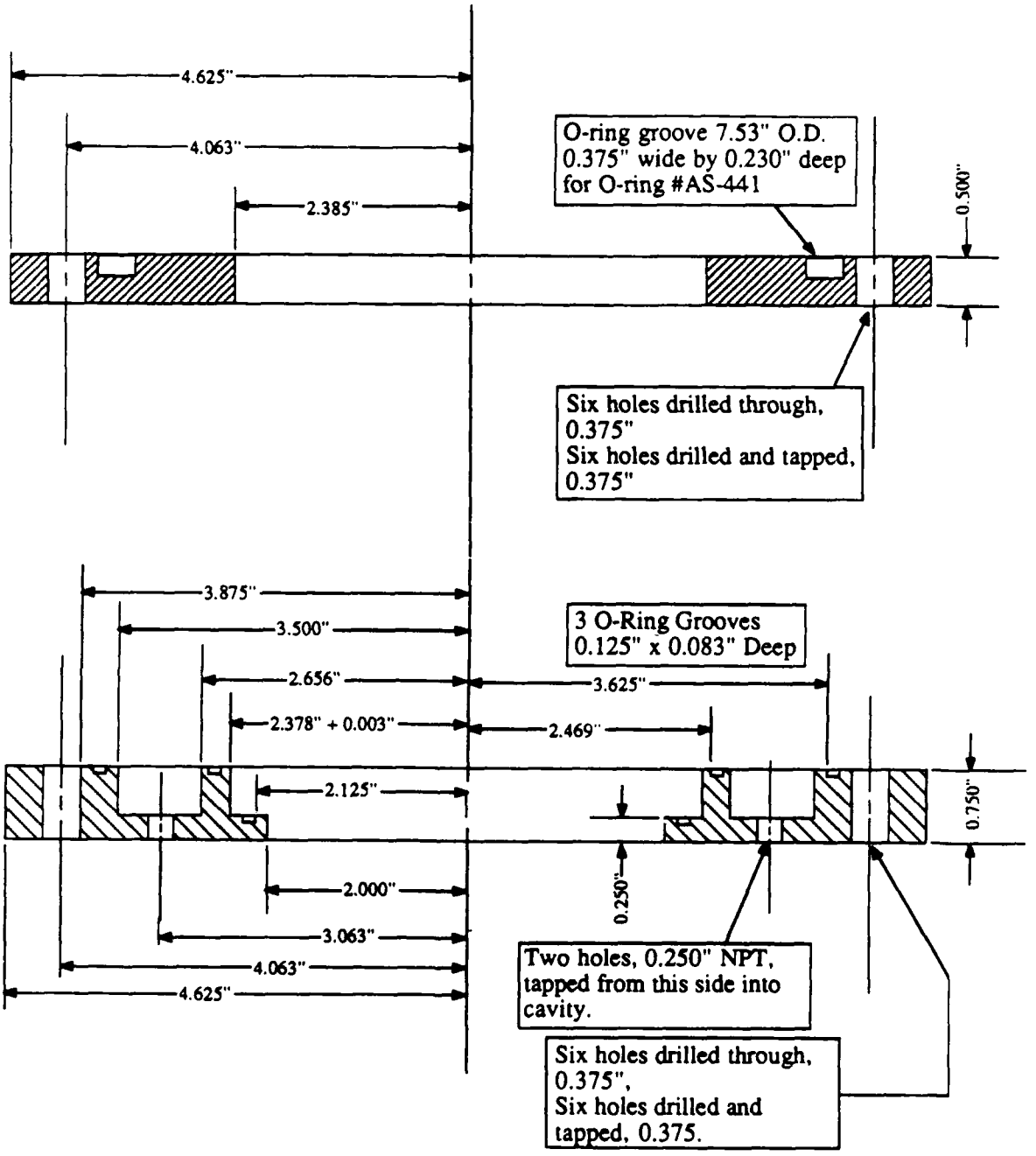

Figure 8.2 Cross sectional view of a water cooled aluminum window holder for zinc selenide or sodium chloride lenses.

END
DATED
FILM
8-88
DTIC